University of West Bohemia

Faculty of Applied Sciences

Ph.D. thesis

2015 **Ing. Michal Meissner**

University of West Bohemia
Faculty of Applied Sciences

REACTIVE MAGNETRON SPUTTERING OF OXIDE BASED AND OXYNITRIDE NANOCOMPOSITE THIN FILMS

Ing. Michal Meissner

Ph.D. thesis submitted to acquire academic title
Doctor of Philosophy
in Plasma Physics and Physics of Thin Films

Supervisor: prof. Ing. Jindřich Musil, DrSc.

Department of Physics

Plzeň 2015

Západočeská univerzita v Plzni
Fakulta aplikovaných věd

REAKTIVNÍ MAGNETRONOVÁ DEPOZICE NANOKOMPOZITNÍCH TENKÝCH VRSTEV NA BÁZI OXIDŮ A OXYNITRIDŮ

Ing. Michal Meissner

Dizertační práce
k získání akademického titulu doktor
v oboru Fyzika plazmatu a tenkých vrstev

Školitel: prof. Ing. Jindřich Musil, DrSc.

Katedra fyziky

Plzeň 2015

Declaration

I hereby declare that I wrote this submitted thesis myself by using the results obtained and published during my Ph.D. study and by using properly cited literature.

Plzeň, 2015 ……

Acknowledgement

I would like to thank to my supervisor prof. Ing. Jindřich Musil, DrSc. for his patient guidance, giving the direction and sharing the ideas for performing a proper science at the Department of Physics, prof. RNDr. Jaroslav Vlček, CSc. for providing me the opportunity for doctoral study and for motivating me, all the friends and colleagues at the department for their friendly attitude and helpful discussions and all the other people helping with obtaining the results presented in this thesis. Last but not least I would like to thank to my mother Marie and my father František and all my friends around who supported me with a patience and motivated me to finish this study.

This work was supported in part by the Ministry of Education of the Czech Republic under Project Nos. MSM 4977751302 and COST OC10045 and in part by the Grant Agency of the Czech Republic GACR under Project No. P108/12/0393.

Contents

1. Introduction

There are increasing demands on products and services with increasing knowledge of the universe and with progressive development of new technologies. With such progress human society requires these products and technologies to be smart, ecologic, cheap, effective and easily reachable like smartphones, considerate waste management, effective use of renewable energy sources, etc. Material sciences dealing with metallurgy, nanomaterials, biomaterials are helping a lot to achieve such goals. Special attention is devoted to thin film and coating technologies based on vacuum and plasma physics. Thin films and coatings are widely used in mechanical engineering in the form of hard and wear resistant coatings, in glass industry as the energy saving windows, in medicine for the antibacterial or biocompatible surface treatment, in aerospace industry due to the thermal, chemical and oxidation resistance, etc. Magnetron sputtering is one of the important and industrially used thin film technology. Thin films based on metals, oxides, nitrides, carbides or composites with unique mechanical, electrical, optical and other properties can be prepared by magnetron sputtering.

This Ph.D. thesis is devoted to the reactive magnetron sputtering of nanocomposite thin films based on oxides and oxynitrides. First part is dealing with two-functional nanocomposite TiO_2/Cu films exhibiting the hydrophilic behaviour together with the antibacterial effect. TiO_2 is well known for its photoactivity namely the UV induced hydrophilicity, photocatalytical decomposition of organic compounds and self-cleaning effect. The addition of selected elements together with the optimization of sputtering process can result in forming of a multifunctional nanocomposite thin film with enhanced properties. Specifically the multifunctionality of materials is one of the progressive directions in material sciences.

Second part of this thesis is dealing with the elimination of arcing during reactive magnetron sputtering of Al_2O_3 films at higher power loads. Arcing is one of the undesired phenomena in reactive magnetron sputtering. Such arcing can cause mainly damaging the growing film. Therefore an optimized stable sputtering process is necessary for the production of quality thin films without defects and it is also important for the developement of high power magnetron systems.

Third part is dealing with the preparation of nanocomposite Al-O-N thin films and their resistance to cracking. Oxynitrides are intensively studied due to a wide range of utility

properties which can be varied by the ratio of oxide and nitride phases and by controlling the film structure from amorphous through nanocrystalline to purely crystalline.

Generally this thesis contributes to the area of multifunctional nanocomposite thin films, the optimization of reactive magnetron sputtering process and the development of hard nanocomposite thin films with enhanced toughness. All these areas are very actuall at the Department of Physics at the University of West Bohemia in Pilsen.

2. Current state of art

2.1. Multifunctional composite thin films

Nowadays multifunctional materials get an increasing attention. Such materials combining mechanical, electrical, optical and other properties are extending their application use in many industries. These materials can be produced by a variety of technologies in the form of bulk, liquid, powder or thin film. Thin film technologies like magnetron sputtering are very promissing for many applications. Considering the main advantages of sputtered thin films like a compact dense structure, good adhesion to the substrate, possibility to produce one-component or composite films prepared at low substrate temperatures [21] this technology is used for the products in semiconductor industry, flexible electronics, aerospace, automotive, healthcare and many other widely spread industries.

Titanium dioxide (TiO_2 or titania) is a valuable material for material research and its application use, see the chapter below. Though the titania is a multifunctional material by itself its combination with other selected materials can either enhance its properties or extend the application use of the resulting composite [30].

2.1.1. Titania and its properties

Titania well-known for its photoactivity exists in three natural forms – brookite, rutile and anatase. The brookite has no significant application use because of its low stability. The rutile is stable at higher temperatures and can be used e.g. as a protective coating or in microelectronics. The anatase gets the greatest attention. It is a low temperature phase and exhibits the UV induced photoactivity, firstly reported by Fujishima [1]. See below the main properties of titania [2-5]:

- high melting point $T_m \geq 1850°C$
- corrosion resistance
- chemical stability
- biocompatibility
- high refractive index: 2.5 for the anatase and up to 2.9 for the rutile

- high transparency for visible spectrum
- absorption of the UV spectrum
- photoactivity induced by the UV irradiation – superhydrophilicity and photocatalytical decomposition

Titania is able to decompose water, organic compounds and even bacteria because of its photoactivity. Mainly the antibacterial effect will be discussed in this chapter. Please refer to the diploma thesis [6] for more information about titania.

2.1.2. Methods for elimination of bacteria

There are several ways how to eliminate the bacteria, see below. Such ways are typically used in hospitals, laboratories, public places or even households.

The **autoclave** [7] is one of the conventional methods. It is used e.g. for sterilizing the surgical instruments where the heat in a high pressure chamber is the main factor of killing the bacteria.

Chemicals used for the disinfection are e.g. chlorine/chlorine dioxide [8] or ethylene oxide. However such chemicals should be handled carefully because of their agresive nature. Also the radicals like hydrogen peroxide H_2O_2, ·OH radical, O_2^- or ozone [9] are very effective in killing the bacteria.

The **UV irradiation** [10] causes the ionisation, excitation and dissociation of atoms or molecules leading to bacterium's death. The UV irradiation has a low efficiency but it can be used as a stimulator in combination with titania, see below.

Microwaves [11] are causing thermal effect, mainly when interacting with water molecules. Such effect kills the bacteria and can be used e.g. for a textile treatment.

Electromechanical effect caused by **pulse electrical field** [12] disrupts bacterium's outer membrane which acts as its first level protection like a skin.

It has also been found that some **metal ions** can harm or cause the death of a bacterium e.g. when a metal atom/ion is digested directly or by stimulating some of the chemical reactions see the Chapter 2.1.3.

Plasma treatment [13] can combine several effects mentioned above, i.e. the UV irradiation, thermal effect or radicals mainly when the oxygen and water are present.

The **titania** is well-known for its photoactivity as already mentioned. When the titania is irradiated by the UV light in the presence of water and oxygen, highly reactive radicals are created with the ability to kill bacteria [14]. Here the ·OH radical is considered to be the most effective one.

The titania can be combined with other elements/compounds either to enhance its antibacterial effect or to add its photoactive behaviour to another material with a different functionality, see below.

2.1.3. Multifunctional titania composites

Composites of titania/metal with enhanced antibacterial effect

Typical antibacterial composites are titania combined with metals where the metal itself exhibits the antibacterial effect [15, 18]. Researchers are focusing mainly the addition of silver or copper into TiO_2 [16, 17].

Silver itself exhibits a strong antibacterial effect. However a dead bacteria cell remains on the silver surface and could be an obstruction for further effective elimination of a living bacteria. On the contrary TiO_2 exhibits a self-cleaning effect. This means TiO_2 can decompose the dead cell mainly to CO_2 and water. This way TiO_2 surface stays clean and ready for further bacteria killing.

Also copper exhibits the antibacterial effect. However the copper itself suffers from a poor corrosion resistance. Therefore the copper has to be used in a form of copper alloys which are generally not effective in bacteria killing in comparison with other antibacterial materials. With respect to this fact composite of copper and titania attracts a great attention.

Mentioned titania/metal composite can be prepared as a very thin metal overlayer on titania. However such overlayer has a very low mechanical durability. More profitable solution is to disperse metal into the titania volume on a atomic/cluster level. Both composites TiO_2/Cu and TiO_2/Ag with a proven antibacterial effect where the metal was dispersed in the volume of a titania film were prepared in the form of nanocomposite thin films by reactive magnetron sputtering and studied at our Department of Physics. More details are reported here [19, 20].

Titania/metal composites can exhibit more than the ability to kill the bacteria. They have also a good optical transparence, good chemical stability and self-cleaning effect

where the self-cleaning effect is profitable for recovering the antibacterial effect on the surface of the film. Moreover its hydrophilic behaviour amplifies the antibacterial and self-cleaning effect. However the preparation method of such multifunctional material has to be well optimized to get such a wide range of properties in one material. Transparent TiO_2/Cu nanocomposite thin films exhibiting both the hydrophilicity and antibacterial effect after UV irradiation will be discussed in more details in the Chapter 5.1.

Reasons describing the enhanced antibacterial effect of TiO_2/Cu composite are listed below:

1. **Titania itself** produces highly reactive radicals like the hydrogen peroxide H_2O_2, ·OH radical or superoxygen O_2^- [22, 23] when irradiated by UV. Here H_2O_2 has two functions: (i) it is directly responsible for killing the bacteria and (ii) it acts as an intermediate product for ·OH production. ·OH radical is considered to be the most effective in photocatalytical decomposition by TiO_2. The lipidperoxidation is considered to be the main mechanism responsible for bacteria´s death in this case [24, 25]. The outer membrane of bacteria consists of lipids which are decomposed by the radicals mentioned above. Such decomposition continues further resulting in harmless products of the reactions like water or CO_2.
2. **Superhydrophilic behaviour** amplifies the titania's photocatalytical activity.

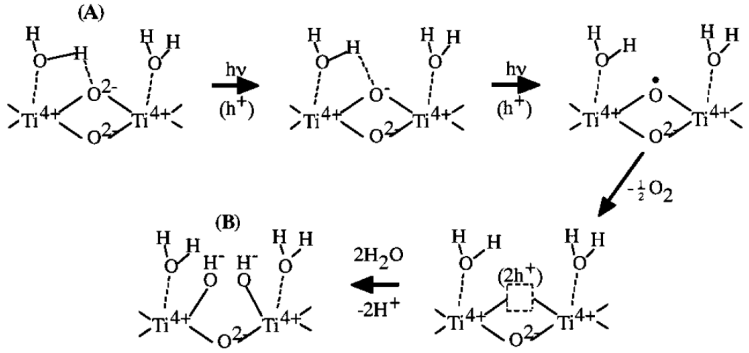

Figure 2.1.1. Schematic illustration of the UV induced hydrophilicity on the TiO_2 surface presented by Sakai et al. in [26].

3. **Copper ion itself** can directly kill a bacterium when endocytosed (i.e. digested) by the bacterium [27].

4. **Copper ion acts as a catalyst** [28] in the water for ·OH production in the presence of H_2O_2. Following chemical reactions illustrate the effect of the copper as an catalyst together with the effect of electron trap.

$$TiO_2 + h\nu \rightarrow TiO_2(e^- + h^+)$$

$$h^+ + H_2O \rightarrow \cdot OH + H^+$$

$$e^- + O_2 \rightarrow \cdot O_2^-$$

$$\cdot O_2^- + e^- + 2H^+ \rightarrow H_2O_2$$

$$Cu^{2+} + e^- \rightarrow Cu^+$$

$$H_2O_2 + Cu^+ \rightarrow \cdot OH + OH^- + Cu^{2+}$$

5. **Copper ion acts as an electron trap**. When the titania is irradiated by UV light, a pair of electron and hole is created. These two particles have a tendency for reverse recombination in a short time. Here the positive copper ion Cu^{2+} captures the electron and the positive virtual hole is free to create the ·OH radical.

Other photoactive titania composites

As already mentioned other materials than metals can be also combined with photoactive titania. An interesting composite is TiO_2/VO_2 [29]. VO_2 varies its infrared transmission with the temperature. It is transparent for IR light at room temperature but this transparency gradually changes to IR reflecting with increasing the temperature. Because VO_2 has a low mechanical durability and moderate chemical stability TiO_2 can be used as a protective and stable overlayer which moreover has a self-cleaning effect in the sunlight. Such a multifunctional composite can be used e.g. in the glass industry or solar applications.

Another example is TiO_2/SnO_2. SnO_2 itself is commercially used in the glass industry as an energy efficient coating [31]. It reflects long IR wavelengths (e.g. from heating

systems or lighting) back to a room. On the other hand it transmits short UV wavelengths. When combined with TiO_2 as an overlayer we get a multifunctional composite coating with the energy saving behaviour and self-cleaning effect.

The colour appearance can be here varied by the thickness of TiO_2 overlayer for both TiO_2/VO_2 and TiO_2/SnO_2 composites.

Other multifunctional thin films with antibacterial effect

Nowadays a great attention is focused on producing the thin composite films exhibiting the antibacterial effect together with a good mechanical durability e.g. TaN/Cu, TaN/Ag [32, 33], Cr-Cu-O [34], ZrN/Ag [35], TiN/Cu [36], etc.

2.2. Elimination of arcing

Reactive magnetron sputtering (RMS) is considered as a very promising technique for producing thin films with unique properties. It is possible to controll the growth of the film structure from amorphous through nanocrystalline to fully crystalline structure either by changing the deposition parameters such as the discharge voltage U_d, discharge current I_d, total pressure p_T, partial pressure of a reactive gas p_{RG}, etc. or by addition of selected elements into the growing film. Such films with controlled structure, parameters and exhibiting multifunctionality can be produced. However RMS suffers from the arcing on a sputtered target, hysteresis and disappearing anode [37, 38, 45, 54, 55]. Therefore the sputtering process has to be well optimized and controlled either to eliminate or at least strongly suppress these undesired phenomena. More details about the RMS, its optimization and perspective can be found for example in these reviews [38 - 42] summarized over the years at our department.

2.2.1. Arcing – origin, consequences and elimination

The arcing is well known and undesired phenomenon accompanying the reactive magnetron sputtering of electrically insulating compounds such as Al_2O_3, MgO, SiO_2, Ta_2O_5, etc. A racetrack of a metallic target is typically free of insulating layer because of the dominant sputtering in this area. Therefore arcing happens preferentially on uneroded areas of the target surface. These areas are coated by products of the sputtering process (depending on the sputtered material and used reactive gas) and their re-sputtering outside the racetrack is typically on a low level if any. As the positive ions are hitting the target surface during the sputtering the positive charge accumulates on the uneroded target surface. Once the accumulated charge achieves a critical value the breakdown occurs due to the arc. Such arc can result in the following undesired events:

- **Instability of the sputtering process**. The process becomes unstable because of the interruption of discharge by switching off the power supply when the arc occurs. Such instability is followed by recovering the deposition process which is in nature strongly nonlinear and it takes some time to recover the process to the original steady state mainly because of the hysteresis phenomenon [43].
- **Damage of a power supply**. The power supply electronics can be damaged due to high current events at the output of the power supply.

- **Damage of the sputtered target.** The target lifetime can be significantly reduced due to a large amount of material released from the target in a form of macroparticles during the arcing.
- **Damage of the growing film.** Growing films are exposed to the impacting macroparticles released from the target during the arcing [44, 45]. Depending on the application these undesired macroparticles in the film can cause (i) the light scattering in optical devices, (ii) short circuits in electronics, (iii) failure of the wear-resistant coatings, (iv) poor adhesion and delamination of the multilayered coatings or (v) oxidation of the corrosion resistant coatings.

There are several ways how to avoid or reduce the arcing [46].

- Arcs can be eliminated by using the **radiofrequency (rf) power supply** for sputtering the compound target e.g. sintered TiO_2 target [47], Al_2O_3 target [48] or ITO target which is used for producing portable biosensing devices, e.g. BioDVD [49].

  Here the defect-free coating is crucial for the functionality of the device. If we consider the BioDVD – device which can detect bacteria or proteins by using the microdiffraction of the laser beam [49] see the schematic illustration in the Figure 2.2.1. The bacterium's typical dimension is 1–10 μm. Considering the unwanted macroparticles which have the same or even bigger dimensions such macroparticles can scatter the light or produce an artificial signal.
- Another way how to eliminate the arcing is to use the **low frequency AC power sputtering** with a single or dual magnetron [56, 57].
- Also modified sputtering system with a **rotatable magnetron** can be used [50, 51]. Rotation of the magnetron ensures that the actuall racetrack is moving on the surface of the target. Therefore less area stays uneroded and coated by the insulating layer resulting in suppression or elimination of the arcing.
- Modifying the system by **obstructing the reactive gas flow on the cathode** [52] or by **controlling the oxygen flow** reported for example by Safi [53] or by Vlček et al. [59] are also very promising techniques.
- The arcing can be eliminated also by using a **pulse power supply (PPS)** [58 – 61] if the repetition frequency f_r is greater than a critical frequency f_{cr}. It

was shown [46] that the critical frequency f_{cr} depends on (i) the discharge current I_d, (ii) pulse-off time t_{off} and (iii) total pressure p_T i.e. f_{cr} = f(I_d, t_{off}, p_T). Based on the experiments where the rectangular single magnetron was sputtered at low target power density $W_{ta} \leq 2$ W/cm^2 it was concluded that the f_{cr} increases with increasing I_d and decreasing t_{off} and p_T. Selection of the correct f_{cr} depends on the charging and discharging processes. However this is not sufficiently investigated so far mainly for higher target power densities $W_{ta} > 10$ W/cm^2.

More details regarding to the elimination of arcing during reactive magnetron sputtering at higher discharge power will be given in the Chapter 5.2.

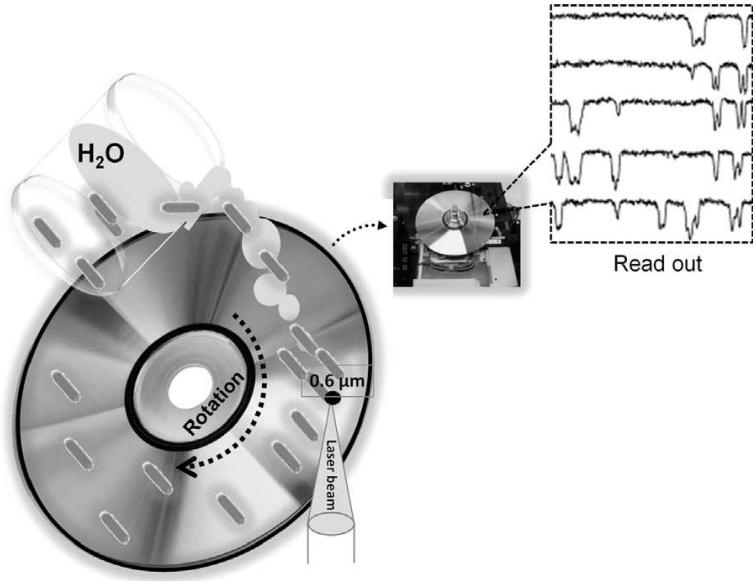

Figure 2.2.1. Schematic illustration of the bacteria detection by laser microdiffraction on BioDVD with sputtered layers [49].

2.3. Oxynitride thin films

Rapidly increasing attention is focused on oxynitrides in last years and specifically to those in the form of thin films. Their application range is versatile due to a tuneable ratio of oxygen/nitrogen content.

2.3.1. Application of oxynitride thin films

Silicon oxynitride (Si-O-N)

Si-O-N films are interesting mainly for the microelectronics, photonics and micro-electronic-mechanical systems (MEMS) due to their high resistivity, high dielectric strength, large band gap and high melting point. Thin Si-O-N films were prepared e.g. by the rf magnetron sputtering of a silicon target in $Ar+O_2+N_2$ mixture [62] or by rf magnetron co-sputtering of Si-O and Si-N targets [63].

Zirconium oxynitride (Zr-O-N)

Zr-O-N films are typically studied due to their photocatalytical activity, for using in polymer electrolyte fuel cells or for producing temperature sensors down to 2 K in high magnetic fields up to 32 T. Rf magnetron sputtering in a water+nitrogen [64] or in $Ar+O_2+N_2$ mixture [65] was used for the preparation of thin films.

Titanium oxynitride (Ti-O-N)

Ti-O-N can be used as a decorative coating due to a tuneable colour and wear resistance or for solar collectors. Pure titanium target was DC sputtered in an $Ar+O_2+N_2$ mixture where the oxygen was introduced in pulses [66]. More details about the reactive gas pulsing process (RGPP) will be given in the Chapter 2.3.2.

Tantalum oxynitride (Ta-O-N)

Ta_2O_5 is used as an antireflection coating or for optical wave-guide devices due to its low absorption, high refractive index and low optical loss. On the contrary TaN is typically used for its hardness and wear resistance. Combining these two materials into a Ta-O-N composite thin film results in a multifunctional material with a tuneable range

of properties depending on the elemental composition. DC RMS of Ta target in $Ar+O_2+N_2$ mixture either with the constant oxygen flow [67] or by using RGPP for the oxygen injection [68] was used to produce Ta-O-N thin films with controlled elemental composition and optical and mechanical properties such as the optical band gap, transmittance, refractive index and stress.

Iron oxynitride (Fe-O-N)

Iron nitride is widely used for magnetic and mechanical applications. On the contrary iron oxides are used in the magnetic storage industry and as catalysts. There is nothing much to say about the Fe-O-N application so far, however Fe-O-N is studied e.g. by Petitjean et al. [69, 70]. Here the films are reactively sputtered from the iron target in a mixture of $Ar+O_2+N_2$ either with a constant or pulse oxygen flow respectively.

Niobium oxynitride (Nb-O-N)

Nb-O-N thin films reactively sputtered either by DC or DC pulse magnetron equipped with Nb target were intensively studied by Fenker, Chappé et al. see [71 – 73]. Oxygen was injected in regular pulses for all their experiments. Nb-O-N film can be used as a topcoat of CrN/NbN coated high speed steels for increasing their oxidation resistance. Also the optical wave-guide application can benefit from this material see the U.S. patent [74]. A quaternary system Ti-Nb-O-N is also suitable for implants as a mechanically durable, wear resistant and biocompatible material [75].

Chromium oxynitride (Cr-O-N)

Chromium nitride is widely used as a protective coating on cutting tools made from high speed steels. Sometimes its structure is stabilized by addition of other elements for reducing the crystallite size resulting in increased thermal and mechanical stability. There has also been an effort to stabilize the structure by addition of the oxygen [76] where the films were reactively sputtered by using rf magnetron. Cr-O-N thin films are also used as temperature-dependent resistors in thermal radiation detectors [77] or as a spectrally selective absorber for photothermal energy conversion [78].

Tungsten oxynitride (W-O-N)

The advantage of the W-O-N is similar to the oxynitrides mendtioned above. It is combining the hardness and wear resistance of the nitride and corrostion resistance of the oxide. Currently reactively sputtered films are studied e.g. by Khamseh [79].

Aluminium oxynitride (Al-O-N)

Al-O-N composite in a bulk form is a very promising material mainly for the military purposes. It is used as a transparent armour for military aircraft, IR and laser windows, hyper-hemispherical domes, military aircraft lenses or scanner windows due to its mechanical and thermal stability and high transparency [80]. Such a ceramic material is typically produced by sintering of AlN and Al_2O_3 powders. The grain size is typically 150–200 μm. Lowering the grain size down to the nanoscale can enhance material properties. This fact is a challenge also for PVD technologies like magnetron sputtering.

Combining the optical, electrical and mechanical properties in Al-O-N composite thin films reveals wide application range e.g. as protective coatings for high speed cutting tools [81], durable optical coatings with high transparency with wide spectral range from UV to mid-IR wavelengths [82], high power density capacitors working at wide temperature range required mainly by military and airspace industry [83], oxygen and water barriers for food industry [84], etc. Also Dreer et al. were studying the preparation of Al-O-N thin films by DC reactive magnetron sputtering of aluminium target in a mixture of $Ar+O_2+N_2$ see the references here [85 – 87].

2.3.2. Reactive gas pulsing process for oxynitride thin film sputtering

Wide range of properties of oxynitride thin films can be controlled by changing the elemental composition i.e. by changing the oxygen to nitrogen ratio in this case. However such a composition controll is not simple when the reactive gases are introduced in a constant flow. Here the oxygen is typically more reactive with the base elements than the nitrogen. Therefore the process has to be well controlled to be able to prepare thin films with a structure from oxide based through oxide/nitride composite to nitride based.

Aronson et al. [88] proposed a new technique where the reactive gas (nitrogen in their study) was introduced in regular pulses during the sputtering of metallic nitride and

oxide films. The idea is to controll the amount of reactive gas so the thin films with a wide range of elemental composition and properties can be prepared.

Even more interesting is using this technique for injecting the oxygen. When a target from metal or other element like silicon is sputtered in a mixture of argon, nitrogen and oxygen the target can be easily poisoned by the oxygen even at low partial oxygen pressure p_{O2} and a thin film with dominating oxide phase will grow. When the oxygen flow is switched on for a defined short time τ_{O2} and then switched off the target state is switching between the oxygen poisoned and the nitrogen poisoned state respectively. Depending on the duty cycle τ_{O2}/T_{O2} the final composition of the growing film can vary from a fully oxide based film through the composite containing both phases of oxide and nitride to a nitride based film. Martin et al. published intensive study on titanium oxynitride thin films reactivelly sputtered from the metallic target by using the oxygen pulsing technique [89 – 95].

Such a way new nanocomposite materials with enhanced properties can be prepared see the chapter below.

2.3.3. Hard thin films with enhanced resistance to cracking

Currently there is a new direction in the development of hard thin films. The focus is on the preparation of thin films with enhanced resistance to cracking under external load [96]. However limited information about such thin films and their testing exists so far and several questions need to be answered e.g. what is the optimum micro-/nano-structure, how is the resistance to cracking influenced by the thickness of the film or by the used substrate, what is the influence of elemental and phase composition and if the high elastic recovery W_e and high ratio $H/E^* > 0.1$ are sufficient conditions to prepare thin films resistant to cracking [97, 98]. Here H/E^* is the ratio of the film hardness H and Young modulus E^*.

First results indicates that the thin films with enhanced resistance to cracking can be found if they exhibit elastic recovery $W_e > 60\%$ and $H/E^* > 0.1$. These conclusions were reported for Zr-Al-O thin films [99], Al-Cu-O thin films [100] and Al-O-N thin films [101] all prepared in our laboratories by reactive magnetron sputtering using the DC pulse dual magnetron. More details on the preparation and testing of Al-O-N thin films are given in the Chapter 5.3.

3. Aims of thesis

The subject of this Ph.D. thesis is the preparation of oxide based and oxynitride thin nanocomposite films by a reactive magnetron sputtering and the characterization of their properties. The Ph.D. thesis is divided in three sections with the following tasks.

1. Two-functional DC sputtered TiO_2/Cu nanocomposite thin films

1. To investigate the optical properties, hydrophilic behaviour and antibacterial effect of DC reactively sputtered TiO_2/Cu nanocomposite thin films as a function of their phase composition and copper content.
2. To find the deposition conditions under which the TiO_2/Cu films are hydrophilic and simultaneously rapidly kill *Escherichia Coli* bacteria after post-deposition UV irradiation.

2. Elimination of arcing in reactive magnetron sputtering of Al_2O_3 thin films

1. To prepare Al_2O_3 thin films by DC pulse reactive sputtering using a single magnetron at different target power densities and different pulse parameters with the aim to find the conditions under which the arcing at the magnetron target can be eliminated.
2. To investigate in detail correlations between the pulse length τ, pulse-off time t_{off}, repetition frequency f_r of pulses, target power density W_{ta} and stability of deposition process and surface morphology of sputtered Al_2O_3 thin films.

3. Two-phase Al-O-N nanocomposite thin films

1. The preparation of Al-O-N thin films by DC pulse reactive sputtering using a dual magnetron in a mixture of oxygen and nitrogen with pulsed oxygen inlet.
2. To investigate in detail correlations between the oxygen pulse parameters, phase and elemental composition and mechanical properties of sputtered Al-O-N films.
3. To investigate the resistance to cracking of sputtered Al-O-N thin films and to find the deposition conditions under which the Al-O-N films resist to cracking in bending.

4. Experimental details

4.1. Deposition system – TiO_2/Cu films

Two-functional TiO_2/Cu nanocomposite thin films were prepared by DC reactive magnetron sputtering using a single unbalanced magnetron.

4.1.1. Vacuum chamber and pumping system

TiO_2/Cu thin films were prepared in a cylindrical vacuum chamber with the diameter Ø = 150 mm and the height h = 245 mm. The chamber made from dural is electrically grounded. Magnetron described in more details in the Chapter 4.1.3. is mounted opposite to a substrate holder. The substrate-to-target distance $d_{S\text{-}T}$ can be varied. Parallelly to the substrate holder a substrate shutter is mounted to cover a sample during stabilizing the deposition process. The substrate holder is electrically isolated from the grounded chamber. Because no bias was applied the substrate was held at the floating potential $U_S = U_{fl}$ during all the discussed depositions. Moreover the substrate holder has a built-in thermocouple for measuring the substrate temperature T_S. Also the holder provides heating of the substrate/sample by a resistance wire. Schematic figure of the described vacuum chamber is in the Figure 4.1.1.

Two basic conditions have to be fulfilled prior to and during the deposition – a low base pressure and high pumping speed. This is provided by:

a) **rotary pump** – used for the pre-evacuation of the vacuum chamber and pre-evacuation of the diffusion pump after venting and for pumping the diffusion pump during the deposition to keep a low operating pressure,

b) **diffusion pump** – used as a main vacuum pump to keep a low pressure and high pumping speed during the deposition.

Technical details on both vacuum pumps are summarized in the following Table 4.1.1.

Table 4.1.1. Basic parameters of the used vacuum pumps

	Rotary pump	**Diffusion pump**
Manufacturer	Alcatel USA	Lavat Chotutice Czech Republic
Pumping speed	20 m^3/h	2000 l/s
Maximum operating pressure	atmosphere	10 Pa

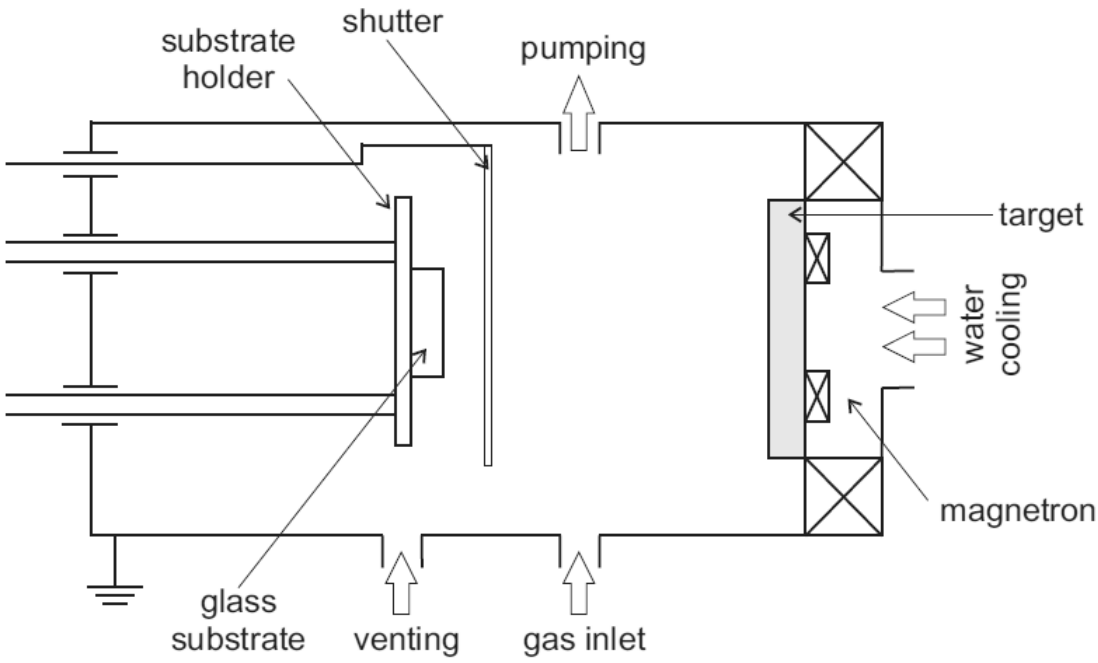

Figure 4.1.1. Schematic illustration of the deposition chamber, single magnetron configuration and substrate holder [103].

Three vacuum gauges are connected to the vacuum system for monitoring the whole pressure range:

1. **Pirani gauge** with its range from the atmospheric pressure down to 5 Pa is used to check the pressure during pre-evacuating the vacuum chamber.
2. **Penning gauge** with its range from $5 \cdot 10^{-1}$ Pa down to $5 \cdot 10^{-6}$ Pa is used for monitoring the base pressure. Base pressure was typically $1 \cdot 10^{-3}$ Pa for all the depositions.

3. **Capacitron gauge** with its range from 13 Pa down to $1 \cdot 10^{-3}$ Pa is used for monitoring the total pressure p_T during the deposition.

4.1.2. Sputtering gas mixture

Two gases were introduced into the vacuum chamber during the deposition. Argon Ar (99.999%) as a working gas and oxygen O_2 (99.999%) as a reactive gas. Both gases were stored in pressure bottles and introduced via a copper manifold into the vacuum chamber. The flow of both gases was controlled via Tesla Rožnov flowmeters. No loop for controlling the total pressure on a constant level was used. Capacitron gauge was set to $1 \cdot 10^{-3}$ Pa once the pumping system reached this base pressure. Then the argon was introduced into the vacuum chamber at $p = p_{Ar}$, the discharge was ignited and the target was cleaned by the discharge during this initial step. Here it is very important to have a substrate covered by the shutter during target cleaning step. Then the oxygen was introduced to achieve desired total and partial pressures, i.e. $p_T = p_{Ar} + p_{O2}$. Once the pressure was stable, shutter above the sample was opened and the deposition started.

4.1.3. Magnetron configuration and power supply

Hybrid electromagnetic unbalanced magnetron shown in the Figure 4.1.2 was used for TiO_2/Cu depositions. The magnetron has an inner electrical coil which varies the electromagnetic field and rectangular permanent Nd-Fe-B magnets on the outer diameter of the magnetron.

The composed Ti/Cu target is shown in the Figure 4.1.3 below. The plane circular target with 100 mm in diameter was made from pure titanium Ti(99.5%) and was fixed to the magnetron by a copper ring and titanium fixing ring. Very limited area of the copper ring covered by Ti fixing ring was facing the discharge allowing only a small amount of copper to be sputtered. Importance of the low copper content in TiO_2 films will be discussed later. Target is directly cooled by water from the open circuit to avoid burning the target sealing and/or damaging the permanent magnets.

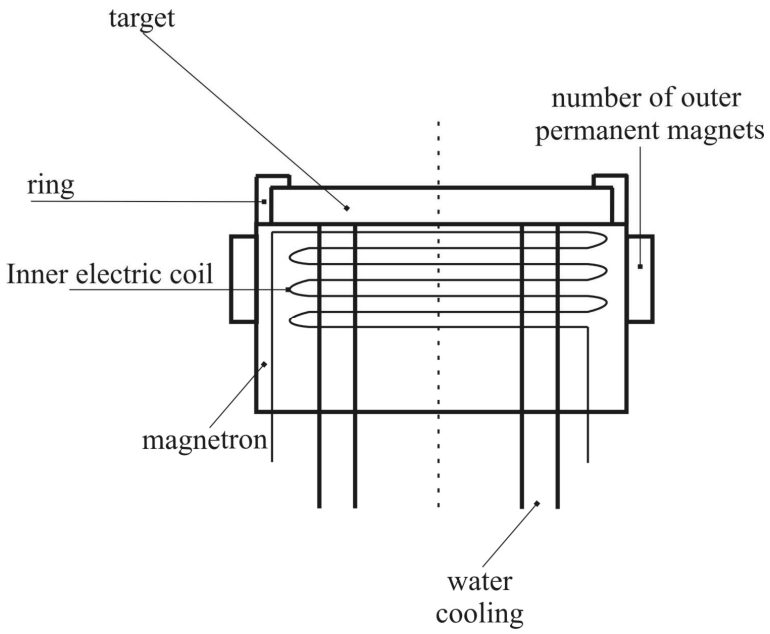

Figure 4.1.2. Schematic drawing of the single unbalanced magnetron [103].

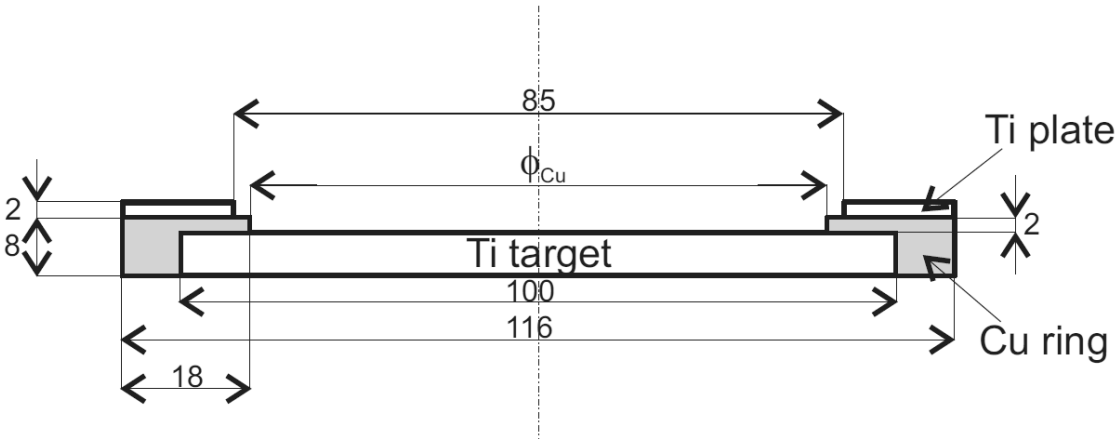

Figure 4.1.3. Schematic drawing of the composed Ti/Cu target used for sputtering composite TiO_2/Cu films. The target is composed of (i) the plane circular Ti target with the diameter ϕ_{Ti}, (ii) copper ring with the inner diameter ϕ_{Cu} and (iii) titanium fixing ring with the inner diameter $\phi_{Ti\,fix}$ [103].

4.2. Deposition system – elimination of arcing

Elimination of the arcing in DC pulse reactive magnetron sputtering of Al_2O_3 thin films prepared by using single unbalanced magnetron was investigated. For this purpose the same deposition system as for Al-O-N thin films was used see the Chapter 4.3. below. The vacuum chamber, pumping system, gas feeding system and PPS were the same as described below. However only the single unbalanced magnetron was used equipped with pure Al (99.5%) target with 100 mm in diameter see the schematic drawing in the Figure 4.2.1. below.

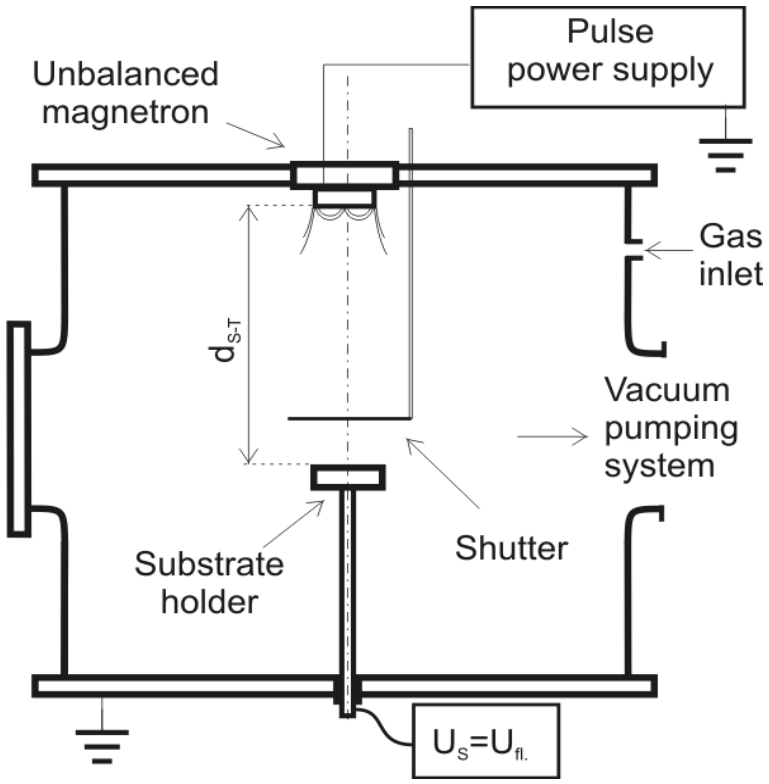

Figure 4.2.1. Schematic illustration of the deposition chamber, single magnetron configuration and substrate holder.

Argon was used as a working gas for cleaning the target by the discharge prior to the deposition. Only the oxygen at the total pressure $p_T = p_{O2} = 1$ Pa was introduced during the deposition process for all the discussed experiments. The oxygen flow ϕ_{O2} was controlled by a feedback loop between Baratron and MKS flow controll unit to keep the constant total pressure p_T during the deposition. One channel of the Advanced Energy

PPS was electrically connected to the single magnetron and the second channel was electrically grounded see the schematic Figure 4.2.2.

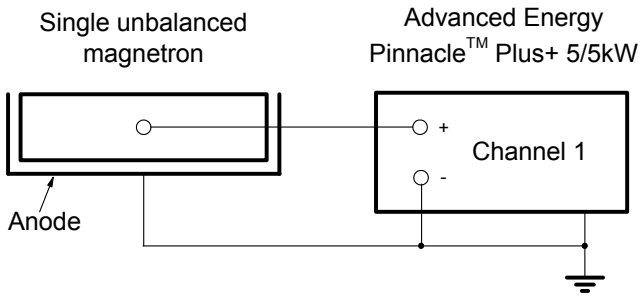

Figure 4.2.2. Schematic illustration of the electrical connection of Advanced Energy pulse power supply to the single unbalanced magnetron.

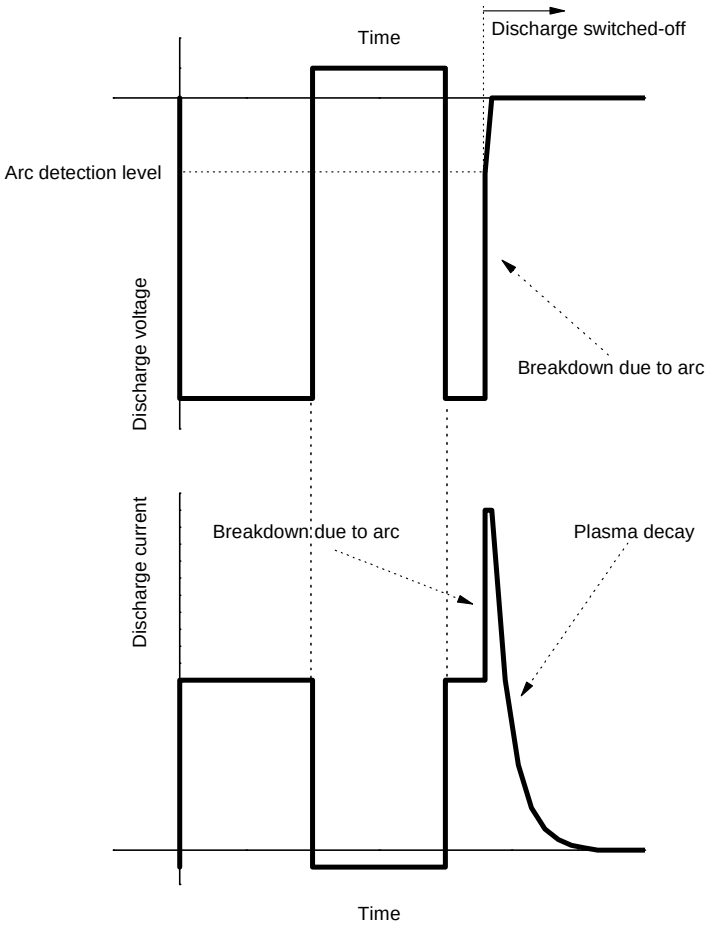

Figure 4.2.3. Schematic illustration of the principle of arc detection feature of Advanced energy pulse power supply.

Arc suppression feature was used for the arc detection and for arc counting to get the quantitative information about the arc occurence. The principle of an arc detection is working on the detection of a sudden voltage drop during the pulse see the schematic Figure 4.2.3. The arc detection level U_{arc} can be manually set to a negative voltage value. Once an arc occurs the current rises up quickly and the voltage drops down quickly. Once the voltage reaches the value of the arc detection level U_{arc} the electronics switches the discharge off and later back on. Every detected arc is counted if the arc detection feature is activated.

4.3. Deposition system – Al-O-N thin films

Al-O-N thin films were prepared by DC bipolar pulse reactive magnetron sputtering using dual unbalanced magnetron equipped with pure aluminium targets sputtered in a gas mixture of nitrogen and oxygen where the oxygen was injected in pulses.

4.3.1. Vacuum chamber and pumping system

Al-O-N thin films were prepared in a cylindrical vacuum chamber with the diameter $Ø$ = 550 mm and the height h = 400 mm. The chamber was made from stainless steel and is electrically grounded. Two magnetrons described in more details below are mounted opposite to a substrate holder but tilted by 20° with respect to the chamber cylindrical axis. The substrate-to-target distance $d_{S\text{-}T}$ can be varied vertically. A shutter is mounted between the targets and the substrate holder for covering the substrate during cleaning the targets in argon discharge and during stabilizing the deposition process. The substrate holder is electrically isolated from the grounded chamber. No bias was applied on the substrate holder during all the discussed depositions. Therefore the substrate was held at the floating potential, i.e. $U_S = U_{fl}$. Moreover the substrate holder has a built-in thermocouple for measuring the substrate temperature. Also the substrate holder provides heating of the sample by a resistance wire up to the maximum possible substrate temperature $T_{S\ max}$ = 500°C. Schematic picture of the described vacuum chamber is shown in the Figure 4.3.1.

Following vacuum pumps were used to achieve low base pressure and high pumping speed:

a) **Rotary pump** is used for the pre-evacuation of the system from the atmospheric pressure down to the operation pressure of the diffusion pump (p < 10 Pa) and to keep a low operation pressure of the diffusion pump during the deposition.

b) **Diffusion pump** is used as a main vacuum pump to keep a low pressure and high pumping speed during the deposition.

Technical details about the vacuum pumps are summarized in the Table 4.3.1. below.

Table 4.3.1. Basic parameters of the used vacuum pumps

	Rotary pump	**Diffusion pump**
Manufacturer	Alcatel USA	Tesla Rožnov Czech Republic
Pumping speed	27 m^3/h	2000 l/s
Maximum operating pressure	atmosphere	10 Pa

Three vacuum gauges are connected to the vacuum system for monitoring the whole pressure range:

1. **Pirani gauge** with its measuring range from the atmospheric pressure down to 10 Pa is used for monitoring the pressure during the pre-evacuation of the vacuum chamber.
2. **Penning gauge** with its range from $5 \cdot 10^{-1}$ Pa down to $5 \cdot 10^{-6}$ Pa is used for monitoring the base pressure. Base pressure was typically $1 \cdot 10^{-3}$ Pa for all the following experiments. The gauge was switched off during the deposition process.
3. **Baratron gauge** with its range from 6.65 Pa down to $1 \cdot 10^{-4}$ Pa is used for monitoring the total pressure p_T during the deposition. The signal from gauge can be also used as a feedback for regulating the gas flow to keep the constant total pressure. However this function was not used for the Al-O-N depositions.

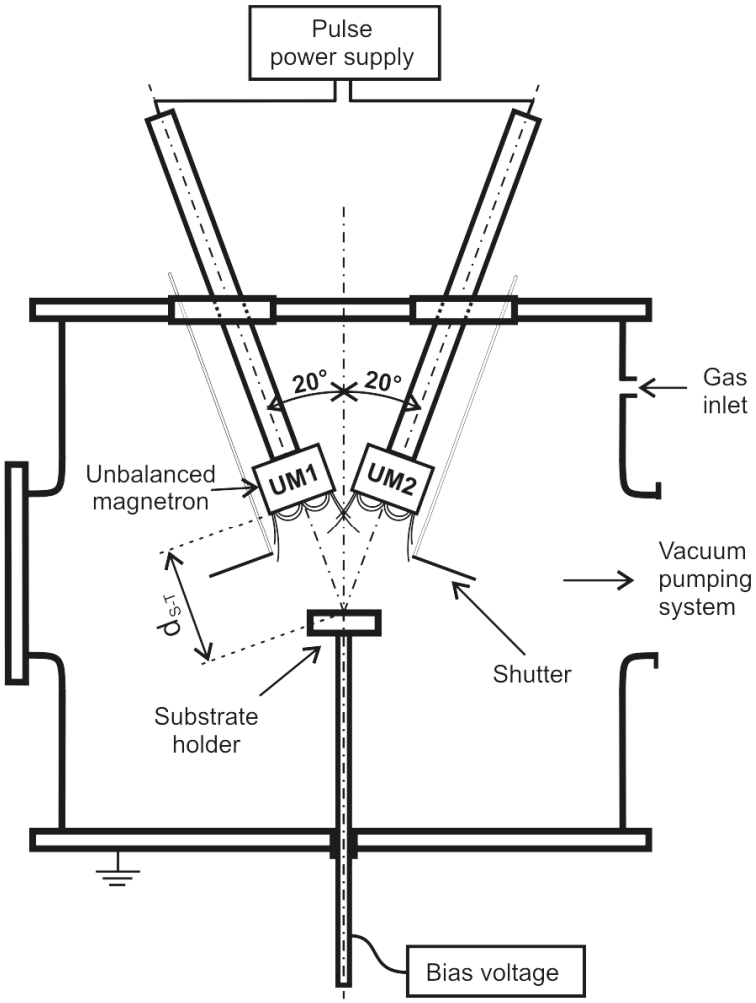

Figure 4.3.1. Schematic illustration of the deposition chamber, dual magnetron configuration and substrate holder.

4.3.2. Sputtering gas mixture

Three gases were introduced before or during the deposition process into the vacuum chamber. Argon Ar (99.999%) as a working gas and oxygen O_2 (99.999%) and nitrogen N_2 (99.999%) as reactive gases. All the gases were stored in the pressure bottles and introduced via the copper manifold into the vacuum chamber. The flow of all the gases was controlled via MKS Mass-Flo Type 1179A flowmeters. There is a possibility to controll the total pressure via the feedback loop on a constant level. However such controll has not been used because of the gas pulsing technique used for Al-O-N

depositions. Gas flows were set and introduced into the vacuum chamber once the pumping system reached the base pressure 0.001 Pa, see the following order of their introduction:

- **Argon Ar** was introduced into the vacuum chamber at ϕ_{Ar} = 20 sccm to get the pressure $p_T = p_{Ar}$ = 1 Pa. The discharge was ignited in Ar and the target was sputter cleaned during this initial step. Here it is very important to have the substrate covered by the shutter. The argon flow was zero during the deposition itself.
- The argon was continuously fully substituted by the **nitrogen N_2** after cleaning the targets in argon plasma while the discharge was still on. Nitrogen flow ϕ_{N2} was optimized to get the total pressure $p_T = p_{N2}$ = 1 Pa in this case at ϕ_{N2} = 27 sccm.
- Third step was to introduce the **oxygen O_2** either at a constant flow (only for limited number of depositions) or in pulses for most of the depositions. This was provided by a computer program which controlled the opening and closing of the oxygen flowmeter for defined times at the defined value of the oxygen flow ϕ_{O2}. Schematic figure of the gas introduction into the vacuum chamber is shown in the Figure 4.3.2.

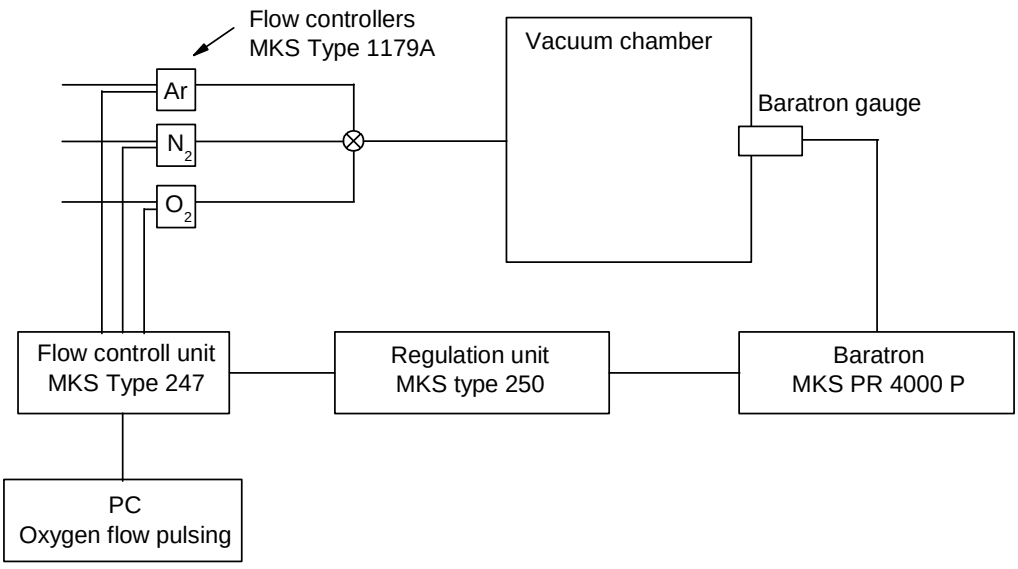

Figure 4.3.2. Schematic illustration of the gas introduction into the vacuum chamber.

4.3.3. Magnetron configuration and pulse power supply

Dual unbalanced magnetron system was used for all the depositions of Al-O-N thin films. Both inner and outer magnets of the magnetrons are permanent Fe-Nd-B magnets with closed magnetic field configuration see the schematic illustration together with the picture of the real discharge in the Figure 4.3.3.

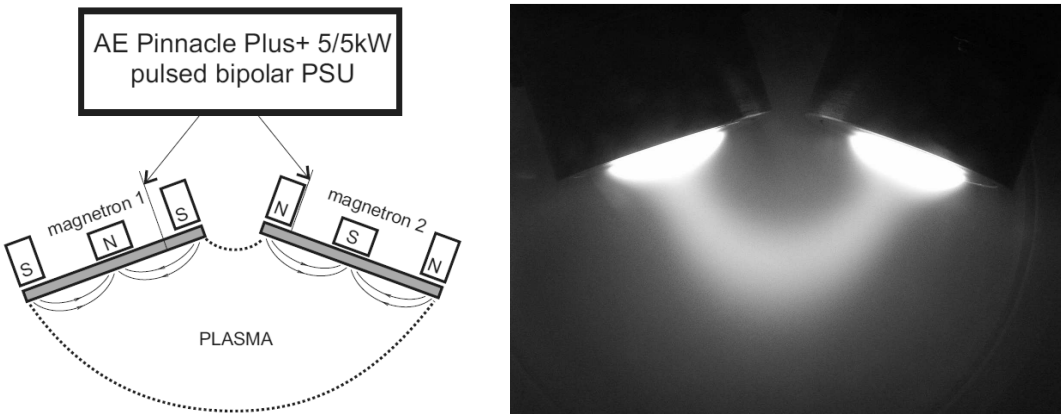

Figure 4.3.3. Schematic illustration of the magnetic field of the used unbalanced dual magnetron (on the left) and picture of the real discharge (on the right).

Targets with 50 mm in diameter shown in the Figure 4.3.4. were made of pure aluminium Al (99.5%). Modification of the plane target (see the cross section in the drawing) is enhancing the plasma confinement in the target surface vicinty see [42] for more details. Targets are directly cooled by water from an open water circuit.

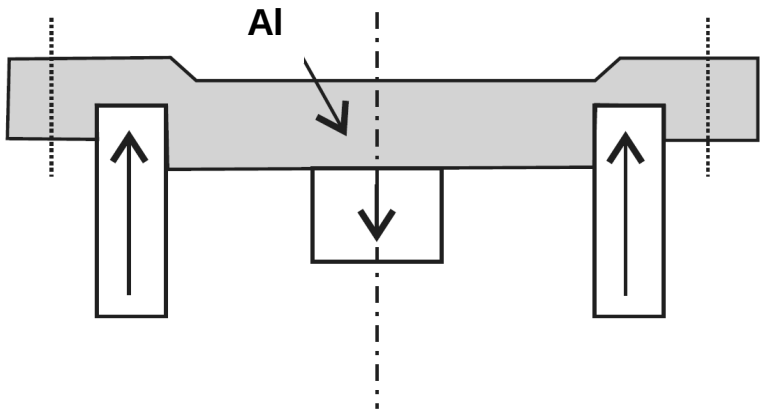

Figure 4.3.4. Schematic drawing of the aluminium target.

The parallel magnetic induction close to the target surface in the racetrack region was ~ 900 G. Such a strong magnetic field allows the efficient plasma confinement in the

target vicinity and higher ion density in comparison to the mirror field configuration. Targets were cleaned by sputtering in pure Ar after pumping down to the base pressure p_0 prior to the deposition. The substrate was covered by the shutter during the target cleaning.

Power applied to the targets was delivered from the two-channel bipolar pulse power supply (PPS) Advanced Energy Pinnacle^{TM} Plus+ 5/5kW. Following Table 4.3.2. summarizes the main parameters of this PPS. The Figure 4.3.5. is representing V-A characteristic of the used Advanced Energy PPS.

Table 4.3.2. Basic parameters of the Advanced Energy PPS.

Parameter	**Value**
Channels	2
Maximum input power P_{in}	5 kW
Maximum discharge current I_{max}	15.5 A
Maximum discharge current U_{max}	650 V
Maximum repetition frequency f_r	350 kHz
Duty cycle τ/T	0.5 – 1.0
Pulse-off time t_{off}	0.4 – 5.0 μs

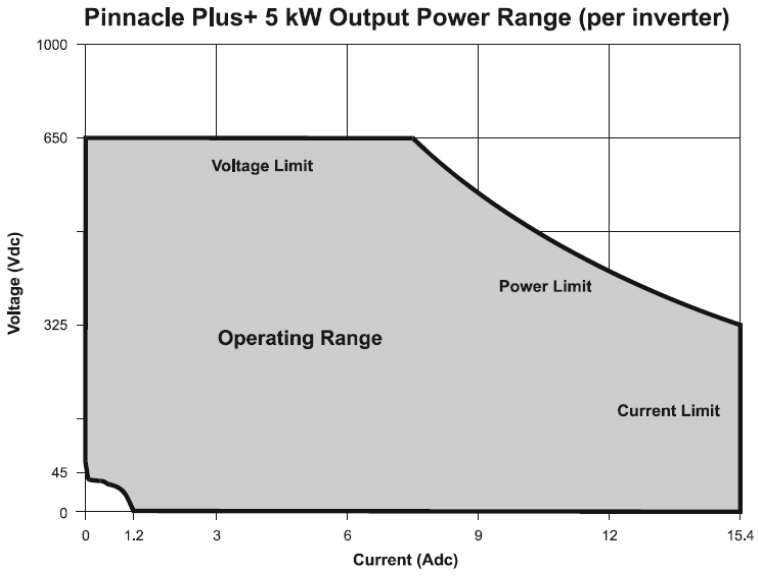

Figure 4.3.5. V-A characteristic of the used Advanced Energy PPS [102].

Both channels can be operated independently. However for all of the Al-O-N depositions so called „dual cathode“ mode was used. The duty cycle is $\tau/T = 0.5$ for both magnetrons in this mode and their phase with respect to each other is shifted by $T/2$. Therefore during each half of the period one magnetron is acting as a cathode and the second one as an anode. Both magnetrons switch their role during the second half of the period. The positive charge accumulated during the pulse on the cathode can be effectively neutralized by the electron flow during the pulse-off time. Such a way stable deposition process at high deposition rates can be performed.

The PPS also has an arc suppression feature. This feature allows the PPS to detect, suppress and count the arc during the reactive sputtering process. This feature was used during the elimination of arcing.

4.4. Thin film characterization

4.4.1. Substrate preparation

Substrate material and dimensions

Following substrate materials were selected for thin film depositions:

1. for TiO_2/Cu thin films: microscopic sodium glass slides 26×26×1mm^3,
2. for Al_2O_3 thin films: Si(100) 20×20×0.38 mm^3,
3. for Al-O-N thin films:
    a. microscopic sodium glass slides 26×26×1mm^3,
    b. Si(100) slides 20×20×0.38 mm^3 and 35×5×0.38 mm^3,
    c. molybdenum stripes 80×15×0.1 mm^3.

Cutting

Glass and silicon substrates were cut by using a diamond tip to desired dimensions from glass slides and silicon wafers respectively. Molybdenum substrates were cut by scissors.

Cleaning

All of the substrates were firstly blowed off with air and manually cleaned with isopropanol to remove the residual macroparticles from the packaging and after the cutting. Then all the substrates were ultrasonically cleaned for 10 minutes in acetone prior to the deposition. Substrates were put into the vacuum chamber after drying in the air flow and the vacuum chamber was pumped down immediately.

Handling and storing

All the substrates prior to the deposition and all the samples after the deposition should be handled cleanly to avoid touching it with a bare hand which can leave a fingerprint on it. Fingerprint is one of the most common contamination sources in the vacuum

systems. Such contamination has a significant effect on the base pressure and quality of the growing film e.g. it can affect the film composition and/or film adhesion to the substrate. Therefore all the samples were handled either with clean tweezers or in vinyl non-powdered gloves.

Samples were stored in polyethylene bags and plastic boxes to keep them from contamination and mechanical damage.

Fixing on substrate holder

Substrates used for the deposition of Al_2O_3 and Al-O-N thin films in dual magnetron system described in the Chapter 4.2. and 4.3. respectively were laid horizontally on the substrate holder without any fixing. Small area of the edge of the substrate was covered to get an uncoated area. The resulting interface between the coated and uncoated area was used for a film thickness measurement after the deposition (see the Chapter 4.4.2. below).

Substrates used for the deposition of TiO_2/Cu thin films were fixed by fixing steel plates vertically on the substrate holder. Area covered by fixing steel plates, i.e. uncoated area was later used for the film thickness measurement.

4.4.2. Film thickness measurement

Thickness of thin films was measured by the Dektak 8 Stylus Profilometer (Veeco, USA) with the accuracy of 1 Å. Here a diamond tip is scanning the surface of the film on the interface between uncoated and coated area of the sample. Thickness of the film is then extracted from the measured profile.

Moreover linear roughness R_a can be evaluated by this equipment from the scanned profile of the thin film.

4.4.3. Phase composition

X-ray diffraction (XRD) was used to determine the phase composition. Diffractometer X'Pert PRO (PANalytical, Netherlands) with Cu Kα radiation (40 kV, 40 mA, λ = 0.154187 nm) working in Bragg-Brentano configuration was used for all the discussed thin films.

4.4.4. Elemental composition

X-ray fluorescence spectroscopy (XRF) was used to determine the elemental composition. XRF Spectrometer MagiX PRO (PANalytical, Netherlands) with rhodium 4 kW radiation source was used for all the discussed experiments.

4.4.5. Hydrophilicity measurement

Determination of the hydrophilic behaviour was carried out for selected TiO_2/Cu thin films by measuring the water droplet contact angle (WDCA) α during the UV irradiation of the films.

UV irradiation system

UV irradiation system made in our laboratories was built for activating the titania films. System consists of 5 UV tubes TL-DK 30W/0.5 (Philips, Netherlands) with λ_{max} = 365 nm. The irradiation power density of the UV system measured at the surface of the thin film is 0.9 - 1.0 W/cm^2. System is air-cooled to avoid the overheating of UV tubes.

WDCA measurement system

WDCA α measurement was performed by using the Surface Energy Evaluation System (SEES) developed at Masaryk University in Brno, Czech Republic. This system connected via USB to the PC consists of the adjustable holder (in *X*, *Y* and *Z* direction), CCD camera for acquiring the images and evaluation software.

All the samples were cleaned by isopropanol prior to the measurement to remove any potential contamination and then dried by air flow because WDCA α can be strongly influenced by any solid particle or liquid remaining on the surface of the thin film.

Water droplet of the volume of 4 μl was applied by precise micropipette Labopette® on the surface of the film at defined time during the UV irradiation. Volume of the droplet was the same for all the WDCA measurements to achieve good reproducibility. Once the droplet was applied on the film surface position of the holder was adjusted to get sharp image with a reasonable size on the screen. Optimizing the light conditions around the sample was important to get good contrast between the droplet and the

background. WDCA α evaluated by the software is here defined as the angle between the tangent of the droplet and the surface of the thin film in their junction.

The measurement error of this system is less than 3% but it increases for WDCA $\alpha \leq 10°$. Thin films exhibiting WDCA $\alpha \leq 10°$ are so called superhydrophilic.

WDCA α measurement was firstly performed prior to UV irradiation and then after defined time steps of UV irradiation. Several droplets were usually applied on the thin film surface and the WDCA α was then determined as the average value at the given time. Here it is important to note that each droplet must be applied on a different place of the film surface to avoid affecting the measurement by previous droplets.

4.4.6. Antibacterial effect evaluation

Antibacterial effect was tested on TiO_2/Cu thin films at the Microbiological institute at Faculty hospital in Pilsen, Czech Republic. UV irradiation system designed in our laboratories was built in the institute for this purpose. System consists of 5 Philips Blacklight UV lamps TL-DK 30W/05SLV (λ_{max} = 365 nm) with power irradiation density of 0.9 – 1.0 W/cm^2 (measured at the level of the thin film surface). Incidentally selected samples of gram-negative *Escherichia Coli* bacteria were used. These bacteria (see the illustrative Figure 4.4.1.) are widely used for such experiments.

Bacteria were diluted in a physiological solution of water and NaCl (0.85% at *pH* = 7.2 at 25°C) with the initial concentration of 10^6 CFU/ml (CFU stands for the Colony Forming Unit). 100μl droplet of this solution with bacteria was then applied on the surface of the thin film and exposed to the UV/VIS irradiation. The droplet was washed down from the sample by 5 ml of physiological solution without bacteria after the irradiation. Volume of 10μl was then spread on Endo agar. This agar is selective microbiological growth medium for most of the gram-negative bacteria. Spread droplet on agar was then cultivated for 24 hours in the microbiological thermostat at 37°C. Grown colonies of the bacteria are clearly visible by naked eye after the cultivation, see the individual round spots in the Figure 4.4.2.

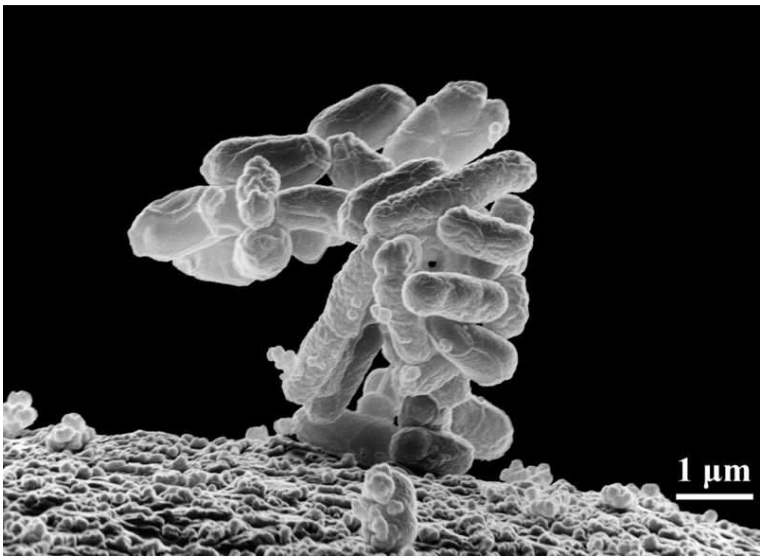

Figure 4.4.1. Illustrative low-temperature electron micrograph of a colony of *Escherichia coli* bacteria [104]. Individual bacterium is oblong shaped.

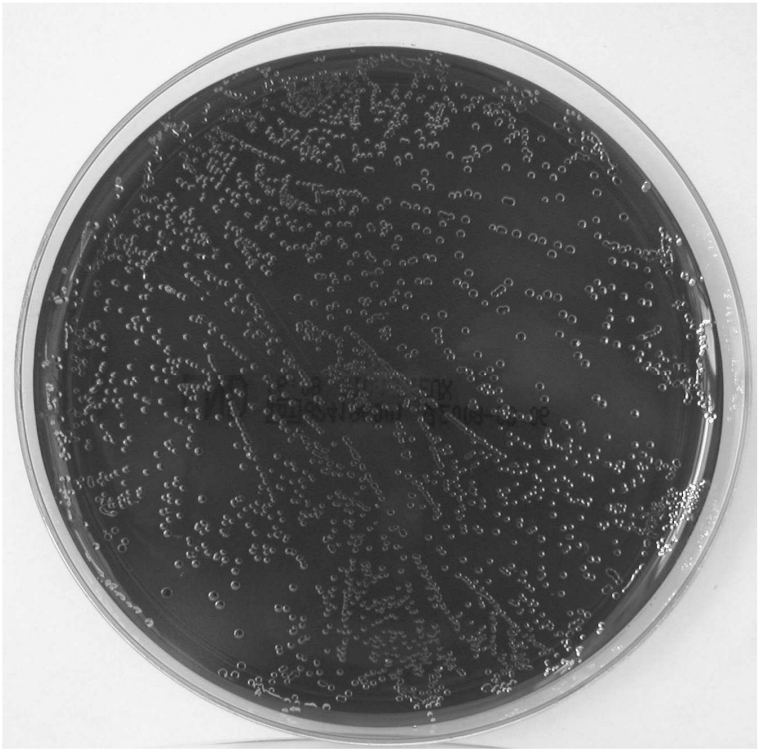

Figure 4.4.2. Picture of bacteria colonies grown on Endo agar after the 24h cultivation at 37°C. Each of the round spots on the agar surface is one bacteria colony.

The experimental setup had to be modified to avoid the evaporation of water from the droplet applied on the thin film surface. Sample was put into the Petri dish with water sodden cotton and covered by the transparent plastic cap. This cap was not affecting the intensity of UV light passing through (confirmed by UV-meter). Such a modification significantly reduces the droplet evaporation. Temperature of the air around the sample was 33°C. All the tested samples were cleaned in acetone as a safety precaution prior to any other handling.

All the samples were tested several times at different arrangements to cover most of the possible factors e.g. TiO_2/Cu films with UV/VIS irradiation, TiO_2 films without Cu, uncoated glass substrate.

4.4.7. Mechanical properties

Vickers indentation method was used for measuring the mechanical properties of Al-O-N nanocomposite thin films discussed in the Chapter 5.3. Computer controlled microhardness tester Fisherscope H100 (Fisherscope) was used for this purpose. Following conditions have to be fulfilled to achieve credible and comparable results:

- Depth of the indentation should not exceed 15% of the film thickness to avoid influence by the substrate.
- Depth of the indentation should be at least 200 nm and/or at least 20*R_a (here R_a is the roughness of the thin film) to reduce the influence of the surface morphology and tip imperfections.
- Several measurements on each sample should be performed to get statistically relevant data. Also each of the measurement position should be in a sufficient distance from the other measurement points and in a sufficient distance from the edge of the film.

The measurement output is so called load curve where the indentation depth is a function of the applied load. Following quantities are extracted from those load curves:

- microhardness H (GPa)
- Young's modulus of elasticity E (GPa)
- depth of the indentation h_{max} (nm)
- elastic recovery W_e (%)

4.4.8. Macroparticle microanalysis

Surface of the selected Al_2O_3 thin films discussed in the Chapter 5.2. were analysed by the scanning electron microscopy (SEM) and by the energy dispersive spectroscopy (EDS). Those thin films were prepared under the stable and unstable conditions. Here the unstable conditions were caused by the arcing during the reactive sputtering when macroparticles were released from the sputtered target. The goal was to acquire the image of those macroparticles on the thin film surface by using SEM Quanta 200 (FEI Company, USA) and to qualitatively evaluate their elemental composition by using EDAX EDS detector (Ametek, USA).

4.4.9. Surface morphology of thin films

Surface morphology of the selected TiO_2/Cu thin films was determined by the atomic force microscopy (AFM) using AFM-Metris-2000 (Burleigh Instruments, USA). Here the Si_3N_4 probe was scanning the TiO_2/Cu film surface in non-contact mode in ambient air and at room temperature. Result is the image of the surface and average surface roughness R_a defined as:

$$R_a = \frac{1}{L}\int_0^L |r(x)|dx$$

where $r(x) = Z(x) - \overline{Z}$. R_a is calculated along the straight line L, typically L = 4 μm. $\overline{Z}$ is the mean height along L.

4.4.10. Optical properties

The optical properties – transmittance $T_{\lambda = 550\ nm}$ and optical band gap E_g – were determined by using the spectrophotometer SPECORD M400 (Carl Zeiss Jena, Germany). TiO_2/Cu thin films deposited on microscopic sodium glass substrates were analyzed by using the spectrophotometer at wavelength range 195 – 700 nm.

Both transmittance $T_{\lambda = 550\ nm}$ and optical band gap E_g were extracted from the measured transmittance spectrum by a Matlab script see the Figures 4.4.3. and 4.4.4. respectively.

Transmittance $T_{\lambda = 550\ nm}$ was evaluated from the spectrum excluding the interference fringes of the film. Interference maxima and minima were fitted by the lines from which $T_{\lambda = 550\,nm}$ is defined as:

$$T_{\lambda=550\,nm} = \frac{T_{\max,\lambda=550\,nm} + T_{\min,\lambda=550\,nm}}{2}$$

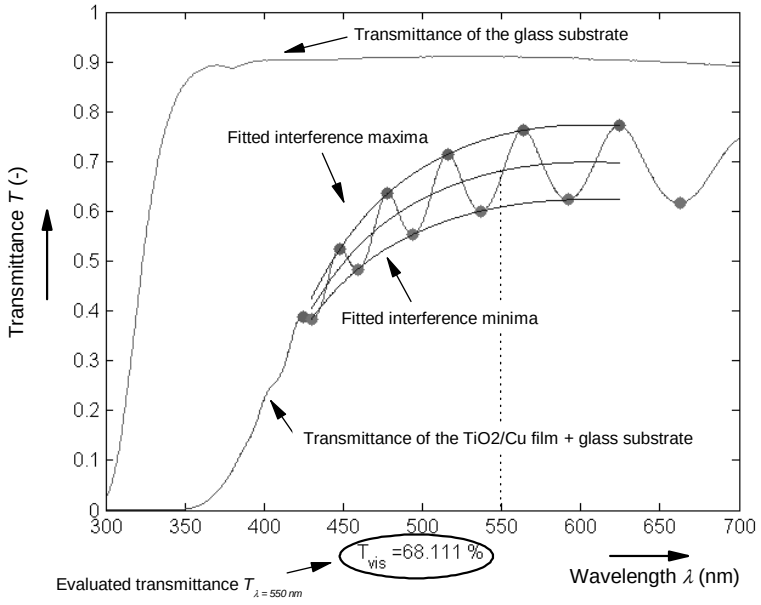

Figure 4.4.3. Illustration of (a) the transmittance spectrum of the glass substrate, (b) transmittance spectrum of the TiO_2/Cu film on glass substrate and (c) evaluation of $T_{\lambda = 550\ nm}$ from the transmittance spectrum of the TiO_2/Cu film on glass substrate.

Measured transmittance data are then converted to the so called Tauc plot where the band gap E_g is determined from the equation [105]:

$$(\alpha h\nu) = B(h\nu - E_g)^p$$

Here h is Planck constant, B is a constant and index p is representing the optical absorption processes listed in the Table 4.4.1.

Table 4.4.1. Index *p* representing the optical absorption processes [105].

Index *p* (-)	**Transition process**
0.5	Direct allowed transition
2	Indirect allowed transition
1.5	Direct forbidden transition
3	Indirect forbidden transition

Indirect allowed transitions are dominant for TiO_2, i.e. p = 2. Quantity α is the absorption coefficient influenced by scattering losses and fundamental absorption. Fundamental absorption dominates over the scattering losses close to the optical band gap E_g. I.e. the absorption coefficient can be determined from the transmittance data as follows:

$$T = e^{-\alpha d}, \text{ i.e. } \alpha = \frac{1}{d}\ln\frac{1}{T}$$

where d is the thickness of the thin film.

Tauc plot for determining the optical band gap E_g is shown in the Figure 4.4.4.

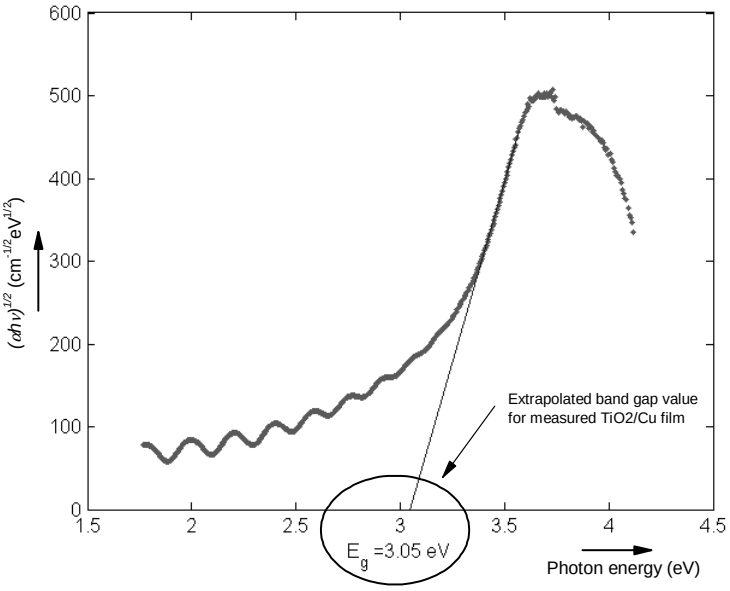

Figure 4.4.4. Illustration of the evaluation of optical band gap value E_g from the transmittance spectrum of the TiO_2/Cu film on glass substrate.

4.4.11. Resistance of thin films to cracking

Currently there is no standard method how to evaluate the resistance to cracking of the thin films. Few methods to assess such resistance are using bending, indentation or scrach test measurements. Bending the thin film on a suitable substrate along a fixed cylinder was used to investigate the resistance of Al-O-N thin films to cracking in this thesis. The resistance of the film to cracking was then assessed from the angle α_c at which the first cracks in the film occured. Good adhesion of the film to the substrate is a crucial condition for using the bending test. Schematic figure of the bending test using the equipment built in our laboratories is shown in the Figure 4.4.5.

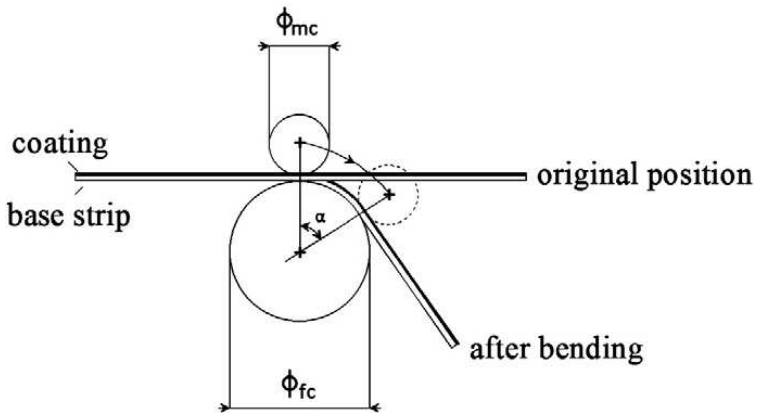

Figure 4.4.5. Schematic illustration of the bending test used to evaluate the resistance of the Al-O-N films to cracking. Here ϕ_{mc} and ϕ_{fc} is the diameter of the moving and fixed cylinder respectively. Angle α is the bending angle.

Al-O-N thin films were sputtered on a Mo-stripe (80x15x0.1 mm^3). Fixed cylinder with the diameter $Ø_{fc}$ = 25 mm was used for all of the measurements. Cracks in the Al-O-N film created after the bending are clearly seen under the light microscope see the illustrative Figure 4.4.6. below.

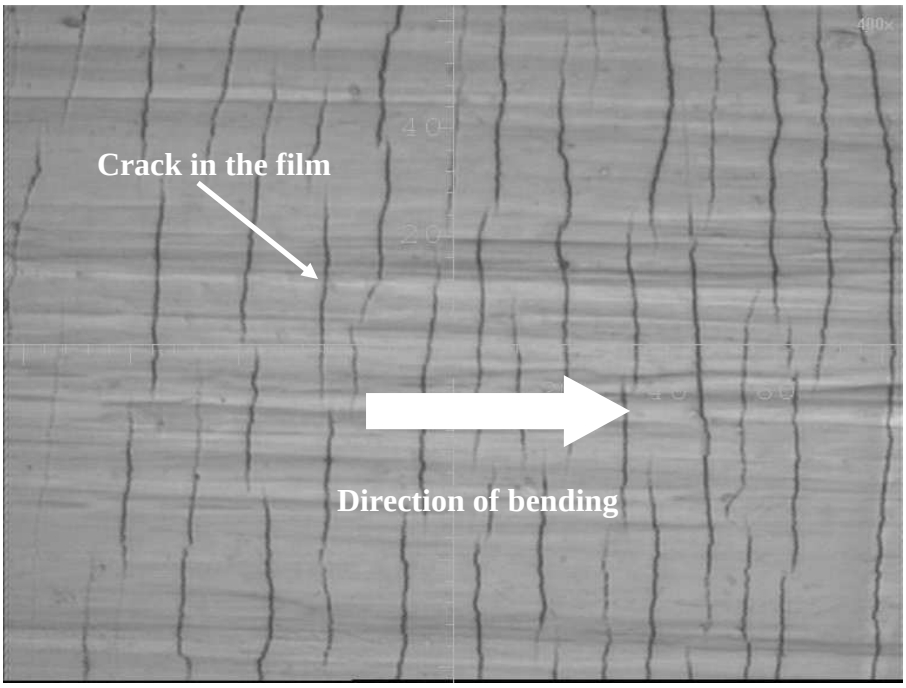

Figure 4.4.6. Micrograph of the cracks in the Al-O-N film on molybdenum stripe acquired by the light microscope. Cracks are perpendicular to the direction of bending.

5. Results and discussion

5.1. Two-functional DC sputtered TiO_2/Cu nanocomposite thin films

Cu-containing TiO_2 thin films were prepared by DC reactive magnetron sputtering using a single magnetron. More details about the deposition system are given in the Chapter 4.1. Deposition conditions used for the preparation of TiO_2/Cu film are summarized in the Table 5.1.1. below.

The aim of this section was to correlate structure and copper content with (i) the UV-induced hydrophilicity and (ii) efficiency of killing of *Escherichia coli* bacteria on the surface of TiO_2/Cu films after UV irradiation. Firstly effect of the deposition conditions and post-deposition thermal annealing on the structure and the optical properties are briefly summarized. Most of the TiO_2/Cu depositions and all the annealing experiments were performed by Václav Ondok and are discussed in more detail in his Ph.D. thesis [103]. Results discussed in this chapter were also published here [19].

Table 5.1.1. Deposition conditions for reactive magnetron sputtering of TiO_2/Cu films

Deposition parameter	**Value/range**
Base pressure p_0	$1 \cdot 10^{-3}$ Pa
Total pressure p_T	0.9 – 2.0 Pa
Partial oxygen pressure p_{O2}	0.9 – 2.0 Pa
Partial argon pressure p_{Ar}	$p_{Ar} = p_T - p_{O2}$
Target-to-substrate distance d_{S-T}	100 mm
Substrate temperature T_S	RT, 300, 400, 500 °C
Substrate potential U_S	$U_S = U_{fl}$ (floating potential)
Discharge current I_d	3 A
Deposition time t_D	100 min
Deposition rate a_D	10 nm/min

Following brief summary about the effect of the copper content in the film, partial oxygen pressure, substrate temperature and post-deposition thermal annealing was

adapted from the thesis [103] for the continuity on the hydrophilicity and antibacterial effect discussed in the Chapters 5.1.1. and 5.1.2.

Effect of copper content in TiO_2 film on structure

Composed Ti/Cu target was used for sputtering the TiO_2/Cu thin films see the Chapter 4.1.3. for more details. The copper content in TiO_2/Cu films was varied by using of the Cu-ring with different inner diameter. It was found out that:

- Increase in the copper content incorporated in the titania matrix up to ~4.5 at.% Cu suppressed the anatase crystallization and in addition rutile crystallization occured. Rutile preferentially grows on impurities and here the copper atoms or clusters can act as the impurity.
- Further increase in the copper content up to 10 at.% Cu suppressed the crystallization completely so the x-ray amorphous TiO_2/Cu composite thin films were sputtered.

Effect of partial oxygen pressure and substrate temperature on structure

Phase composition can be controlled by varying the partial oxygen pressure p_{O2}. Increase in p_{O2} promotes the anatase phase crystallization due to the presence of sufficient amount of oxygen needed for forming the stoichiometric anatase phase. Simultaneously the rutile crystallization is not affected significantly if the substrate temperature T_S is not changed.

On the other hand increase in T_S promotes rutile crystallization by increasing the energy delivered to the growing film.

Both effects of p_{O2} and T_S are illustrated in the Figure 5.1.1. below where the XRD patterns of selected TiO_2/Cu films are presented accompanied with their optical properties.

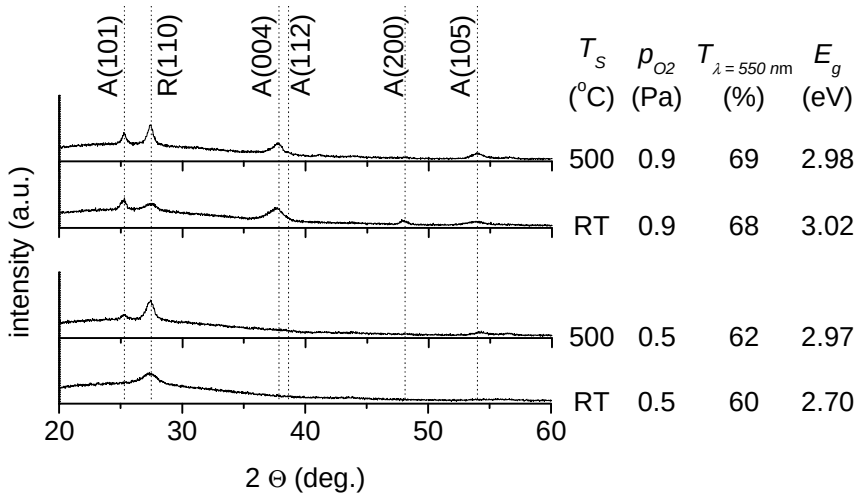

Figure 5.1.1. XRD patterns and optical properties of ~ 1 μm thick TiO_2/Cu films with ~ 4.5 at.% Cu sputtered on glass substrate at I_d = 3 A, $d_{S\text{-}T}$ = 100 mm, $U_S = U_{fl}$, p_T = 0.9 Pa and different partial oxygen pressure p_{O2} and different substrate temperature T_S.

Effect of post-deposition thermal annealing

Amorphous TiO_2/Cu thin films with a different Cu-content where thermally annealed in vacuum and oxygen up to 500°C. It was found out that:

- TiO_2/Cu films thermally annealed in vacuum up to 500°C remained x-ray amorphous.
- The nanocrystallization of TiO_2/Cu films with lower Cu-content up to ~4.6 at.% can be achieved when annealed in oxygen.
- Thermal annealing at the given conditions (p_{O2} = 10 Pa, T_a = 500°C and t_a = 60 min) is insufficient for stimulating the crystallization of amorphous TiO_2/Cu films with higher Cu-content ~10 at.%.
- Post-deposition thermal annealing can be used to controll the final optical properties like transmittance T and optical band gap E_g.

The effect of the thermal annealing (both in vacuum and oxygen atmosphere) on the structure and optical properties is illustrated in the Figure 5.1.2. below.

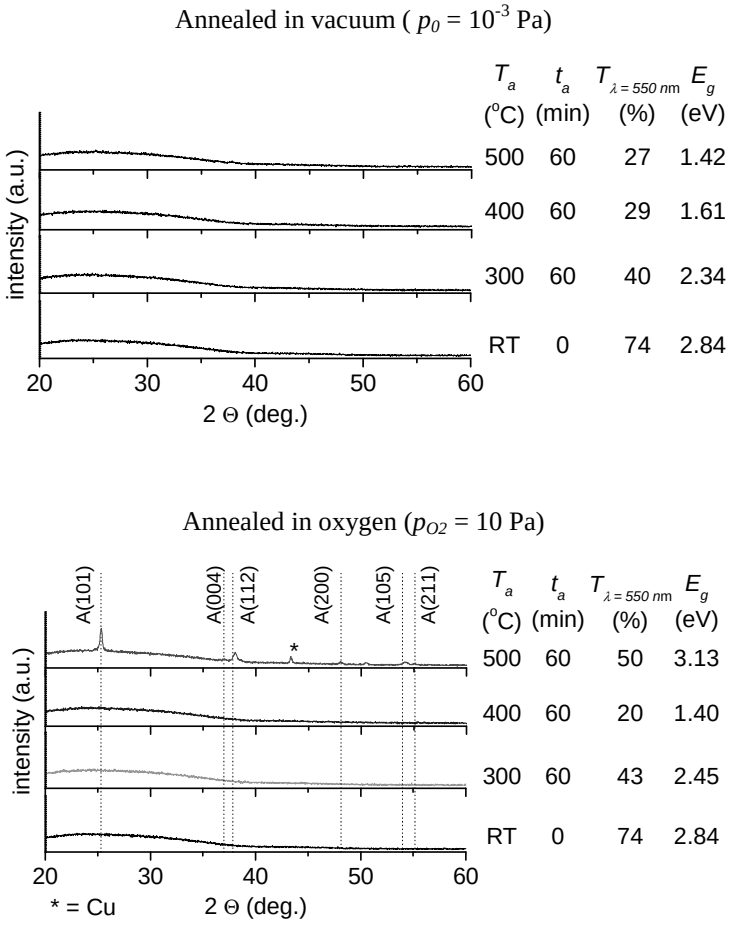

Figure 5.1.2. XRD patterns of ~ 1 μm thick TiO_2/Cu film with ~ 4.5 at.% Cu thermally annealed in vacuum (at $p_0 = 10^{-3}$ Pa) and oxygen (at p_{O2} = 10 Pa). As-deposited film was sputtered on unheated glass substrate at I_d = 3 A, $d_{S\text{-}T}$ = 100 mm, $U_S = U_{fl}$, p_T = 2.0 Pa and p_{O2} = 0.5 Pa.

5.1.1. UV-induced hydrophilicity of TiO_2/Cu films

The hydrophilicity of TiO_2/Cu films was induced by ultraviolet irradiation and evaluated by measuring the water droplet contact angle α (WDCA) during the time of UV irradiation. Both irradiation and evaluation systems are described in the Chapter 4.4.5. Hydrophilicity of four selected TiO_2/Cu thin films prepared at different deposition conditions exhibiting different structure is discussed below.

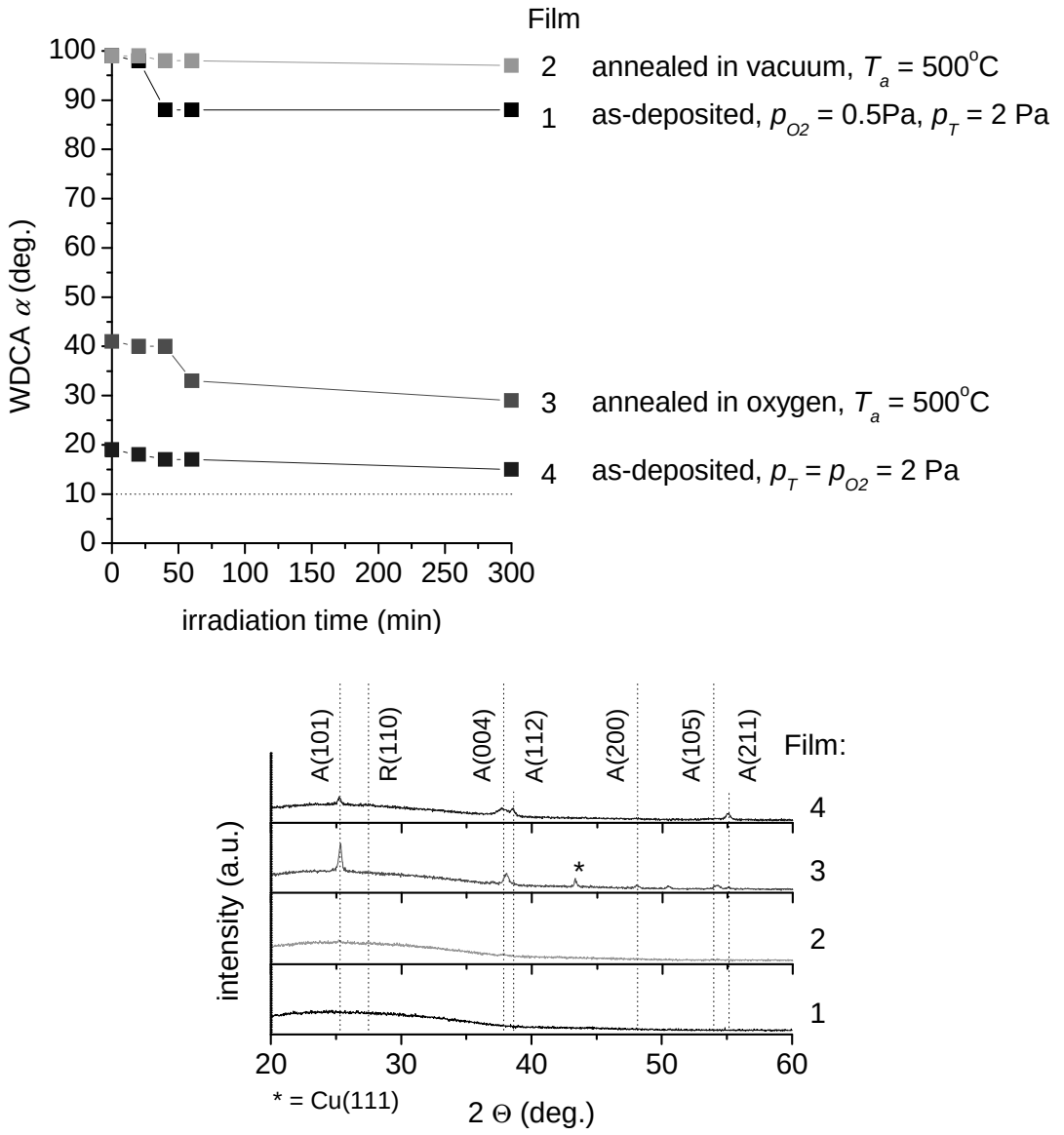

Figure 5.1.3. WDCA α and XRD patterns of selected TiO_2/Cu thin films.

The Figure 5.1.3. shows XRD patterns of the selected TiO_2/Cu films and the evolution of WDCA α during the time of UV irradiation. Following can be concluded:

- Thin films with x-ray amorphous structure either deposited on unheated substrate or annealed in the vacuum (see the films no.1 and no.2 respectively)

exhibit high WDCA $\alpha \approx 100°$ before UV irradiation and negligible decrease of α after 300 min of UV irradiation. Copper content in these two films is 5.1 and 4.4 at.% respectively.

- Samples with nanocrystalline anatase structure (film no.3) and nanocrystalline anatase+rutile structure (film no.4) both exhibit low WDCA α after the UV irradiation. As-deposited film no.4 exhibit low WDCA even before the UV irradiation and there is negligible decrease after 300 min of UV irradiation. This negligible decrease is not clear and it needs further investigation which is however out of the scope of this thesis.

Information about the structure of these selected thin films together with optical properties, WDCA values and surface roughness values are summarized in the following Table 5.1.2. The roughness was measured by the atomic force microscopy (AFM) and surface morphology of each sample is shown in the Figure 5.1.4.

Table 5.1.2. Summary of the structure, optical properties, WDCA α and roughness R_a of the selected TiO_2/Cu thin films.

Film no.	Structure	E_g (eV)	$T_{\lambda=550nm}$ (%)	$\alpha_{0\ min\ UV}$ (°)	$\alpha_{20\ min\ UV}$ (°)	$\alpha_{300\ min\ UV}$ (°)	R_a (nm)
1	amorphous	2.45	43.0	99	98	88	0.5
2	amorphous	1.42	27.0	99	98	97	0.2
3	nanocrystalline	3.13	49.7	41	40	29	6.1
4	nanocrystalline	3.06	66.0	19	18	15	1.4

Films no. 3 and no. 4 with nanocrystalline structure exhibit higher value of the optical band gap E_g = 3.13 and 3.06 eV respectively in comparison with amorphous films no. 1 and no. 2 which exhibit E_g = 2.45 and 1.42 eV respectively. Higher value of E_g is caused by the presence of crystalline phase in the film.

Films no. 2 (annealed in vacuum) and no. 3 (annealed in oxygen) both contain 4.5 at.% Cu and were both deposited at p_T = 2 Pa and p_{O2} = 0.5 Pa. Nanocrystalline film no. 3 annealed in oxygen exhibits higher values of E_g and T in comparison with the amorphous film no. 2 annealed in vacuum. Higher values of the optical properties of the film no. 3 are caused by forming of crystalline stoichiometric structure.

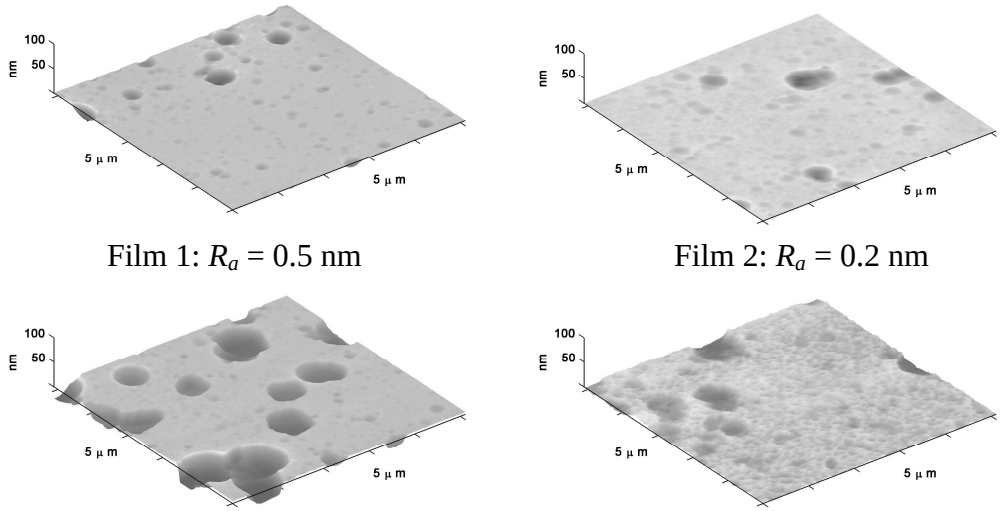

Film 1: R_a = 0.5 nm Film 2: R_a = 0.2 nm

Film 3: R_a = 6.1 nm Film 4: R_a = 1.4 nm

Fig. 5.1.4. Surface morphology and surface roughness R_a of TiO_2/Cu films denoted as films 1, 2, 3 and 4 measured by AFM.

5.1.2. Antibacterial effect

Pure titania film, TiO_2 films with different copper content and pure glass substrate were tested with and without UV irradiation. This way the effect of material, its structure, copper content, type and time of irradiation can be distinguished. Following conclusions regarding to the antibacterial effect were found.

- **No measurable bacteria killing, i.e. massive bacteria growth after the cultivation**

  Several cases were found out when no measurable bacteria killing was observed. Such situation is represented by the Figure 5.1.5. where the massive growth of *E.Coli* bacteria colonies after the cultivation is clearly seen. Such cases were found for:

  - *Bacteria on a clean glass substrate irradiated by UV irradiation for 60 min*

    Amorphous soda lime glass used as a typical substrate for sputter deposition of TiO_2/Cu thin films does not have enough electrochemical potential to form any of the reactive radicals under UV/VIS irradiation to

decompose organic compounds from which bacteria cell consists of. This experiment also showed that the UV irradiation system used in our experiments is not strong enough to kill bacteria by itself. This is very important fact which helps to better distinguish between different factors influencing the bacteria killing.

- *Bacteria on amorphous TiO_2/10 at.% Cu film irradiated by UV for 20 min*

  No measurable bacteria killing was observed on the surface of x-ray amorphous TiO_2/Cu film with higher Cu-content. Amorphous titania films generally exhibit negligible or no UV-induced photocatalytic decomposition.

- *Bacteria on anatase TiO_2/1.5 at.% Cu film irradiated by visible room light for 60 min*

  Daylight inside the laboratory where the antibacterial effect was tested has not enough power to activate the photocatalytic process on the surface of crystalline anatase film.

Figure 5.1.5. Picture illustrating no measurable killing of *Escherichia coli* bacteria exposed to UV/VIS irradiation on TiO_2/Cu film or glass substrate surface where the irradiation was followed by cultivation for 24 h at 37°C on Endo agar covering the Petri dish.

- **Very weak bacteria killing, ~10^3 viable cells**

  This situation is represented by the Figure 5.1.6. which was considered by microbiological specialist as a visible killing effect but very weak.

- *Bacteria on amorphous TiO_2/10 at.% Cu film irradiated by UV for 60 min*

  It was mentioned above when such sample is UV irradiated for 20 min no measurable killing is observed. However there is very weak killing observed (~10^3 viable cells) after 60 min of UV irradiation. Because the used UV irradiation itself was considered as harmless to the living bacteria the explanation can be a relatively high amount of the copper in the titania film. It is known that the copper itself exhibits antibacterial effect. Here the weak killing rate can be due to a low active area of the copper atoms/clusters on TiO_2/Cu surface.

- *Bacteria on crystalline anatase TiO_2 film without incorporated copper irradiated by UV for 60 min*

  Crystalline and pure TiO_2 film with anatase phase does not have to be a sufficient condition for killing the *E. coli* bacteria. It was found out that the killing efficiency of *E. coli* bacteria was very weak in this case. The reason of such weak killing rate can be the fast recombination of the created electron-hole pairs i.e. low amount of created reactive radicals.

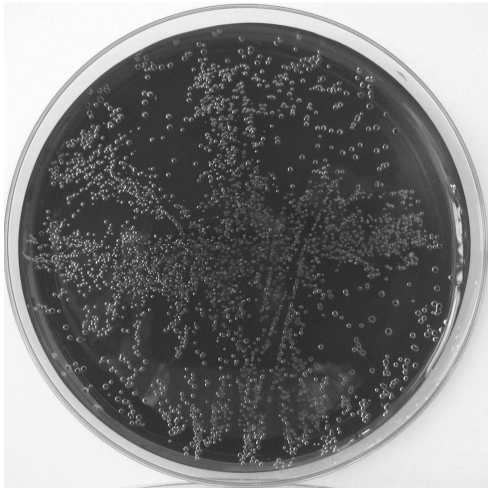

Figure 5.1.6. Picture illustrating very weak killing efficiency of *Escherichia coli* bacteria exposed to UV irradiation on TiO_2/Cu or TiO_2 film surface where the irradiation was followed by cultivation for 24 h at 37°C on Endo agar covering the Petri dish.

- **Weak bacteria killing, ~10^2 viable cells**

  Figure 5.1.7. shows *E. Coli* colonies after the cultivation when weak bacteria killing occured.

  - *Bacteria on crystalline TiO_2/4.5 at.% Cu film irradiated by UV for 60 min*

    Here the weak killing was observed for those films exhibiting crystalline structure either with rutile or rutile+anatase where the rutile was dominating. Such films were prepared at p_T = 0.9 Pa on unheated substrate and substrate heated at T_S = 500 °C respectively. Here the crystalline photoactive structure together with the copper acting as electron trap are responsible for killing the bacteria. However, in comparison with the following results, dominating rutile phase is not photoactive enough to kill all the living bacteria in the solution at the given conditions.

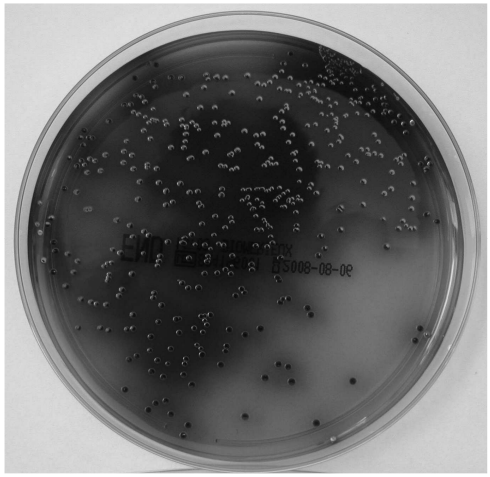

Figure 5.1.7. Picture illustrating weak killing efficiency of *Escherichia coli* bacteria exposed to UV irradiation on TiO_2/Cu film surface where the irradiation was followed by cultivation for 24 h at 37°C on Endo agar covering the Petri dish.

- **Strong bacteria killing, no viable cells**

  Strong bacteria killing is represented by no grown bacteria colonies after the cultivation, see the Figure 5.1.8.

- *Bacteria on anatase crystalline TiO_2/1.5 at.% Cu film irradiated by UV for 20 min*

  It was found out that very fast killing of bacteria occured after 20 min of UV irradiation on the surface of anatase TiO_2 film with low amount of incorporated copper in this case 1.5 at.%.

Figure 5.1.8. Picture illustrating strong killing efficiency of *Escherichia coli* bacteria exposed to UV irradiation on TiO_2/Cu film surface where the irradiation was followed by cultivation for 24 h at 37°C on Endo agar covering the Petri dish.

Good reproducibility was confirmed for all the cases above by repeating the tests several times.

Based on the findings above following can be concluded. Optimum between the deposition conditions, copper content and structure has to be found for producing the thin films capable of effective bacteria killing in a short time. We have found out that anatase TiO_2/Cu nanocomposite thin film with 1.5 at.% Cu sputtered on unheated substrate at $p_T = p_{O2} = 2$ Pa exhibits such behaviour. Simultaneously this film also exhibits good UV-induced hydrophilicity with WDCA $\alpha \leq 20°$. In other words two-functional nanocomposite thin film exhibiting both antibacterial effect and hydrophilic behaviour was prepared which is the key result of this research.

5.2. Elimination of arcing in reactive magnetron sputtering of Al_2O_3 thin films

This section reports on elimination of arcing during DC pulse reactive magnetron sputtering of Al_2O_3 thin films. The unbalanced single magnetron equipped with aluminium target was used for the experiments. The target was sputtered in a pure oxygen atmosphere at relatively high target power density W_{ta} ranging between 10 – 50 W/cm^2. Here the W_{ta} is the averaged target power density over the pulse.

Arcing during the reactive magnetron sputtering is one of the undesired phenomenon which causes instability of the deposition process accompanied by damaging the growing film by macroparticles released from the target when an arc occurs. Such arcs need to be eliminated or at least strongly suppressed.

Correlations between the repetition frequency f_r, pulse-off time t_{off} and its transient phenomena and arcing are discussed in detail. It is shown that the target power density W_{ta}, pulse-off time t_{off} and its transient phenomena are of key importance for the elimination of arcing.

5.2.1. Deposition conditions

Experimental setup is described in the Chapter 4.2. Deposition conditions and pulsing parameters are summarized in the following Table 5.2.1.

Schematic electrical connection and schematic time evolution of the discharge voltage are shown in the Figure 5.2.1. The schematic electrical connection shows only a connection of one channel of the PPS. The second channel was not used and was electrically grounded during all the experiments.

Table 5.2.1. Summary of the deposition conditions and pulsing parameters of the Advanced Energy PPS.

Parameter	Value	Notes
Total pressure $p_T = p_{O2}$	1 Pa	
Substrate-to-target distance $d_{S\text{-}T}$	100 mm	
Target power density W_{ta}	10 – 50 W/cm^2	[1]
Repetition frequency f_r	5 – 100 kHz	[2]
Pulse-off time t_{off}	0.4 – 5.0 μs	[3]
Duty cycle τ/T	50 – 99.8 %	
Arc detection level	-50 and -100 V	[4]

Notes:

[1] W_{ta} = 50 W/cm^2 is the maximum target power density which is possible to deliver by the used system configuration.

[2] f_r = 5 kHz is the minimum repetition frequency of the used Advanced Energy PPS.

[3] t_{off} = 0.4 μs is the minimum pulse-off time of the used Advanced Energy PPS for the whole repetition frequency range.

t_{off} = 5.0 μs is the maximum pulse-off time for f_r = 100 kHz because the minimum allowed duty cycle is τ/T = 50%.

[4] The arcs were detected, counted and suppressed by the PPS. For most of the experiments the detection level was set at -50 V, for one specific experiment also -100 V was used see the chapter 5.2.7.

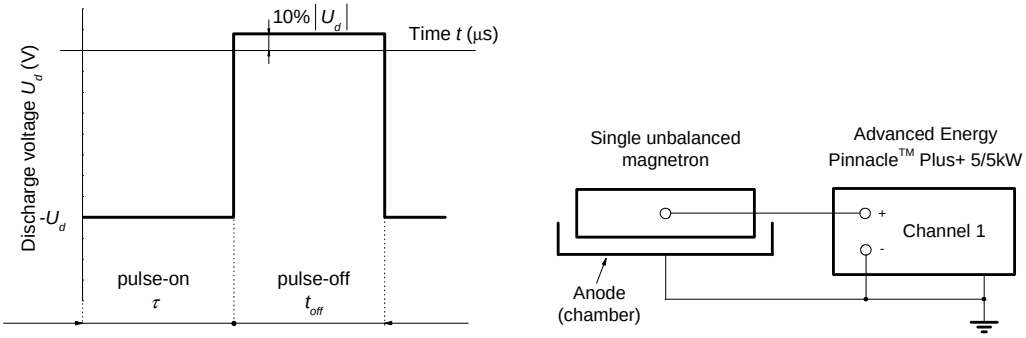

Figure 5.2.1. Schematic illustration of (a) the time evolution of the discharge voltage $U_d(t)$ and definition of pulse-on and pulse-off time and (b) electrical connection of Advanced Energy pulse power supply to single unbalanced magnetron.

5.2.2. Effect of pulse-off time t_{off} on process stability

Different pulse-off times t_{off} were applied for different repetition frequencies f_r. Strong difference in transient phenomena for both the discharge voltage U_d and discharge current I_d at high W_{ta} = 50W/cm^2 were found, see the Figure 5.2.2.

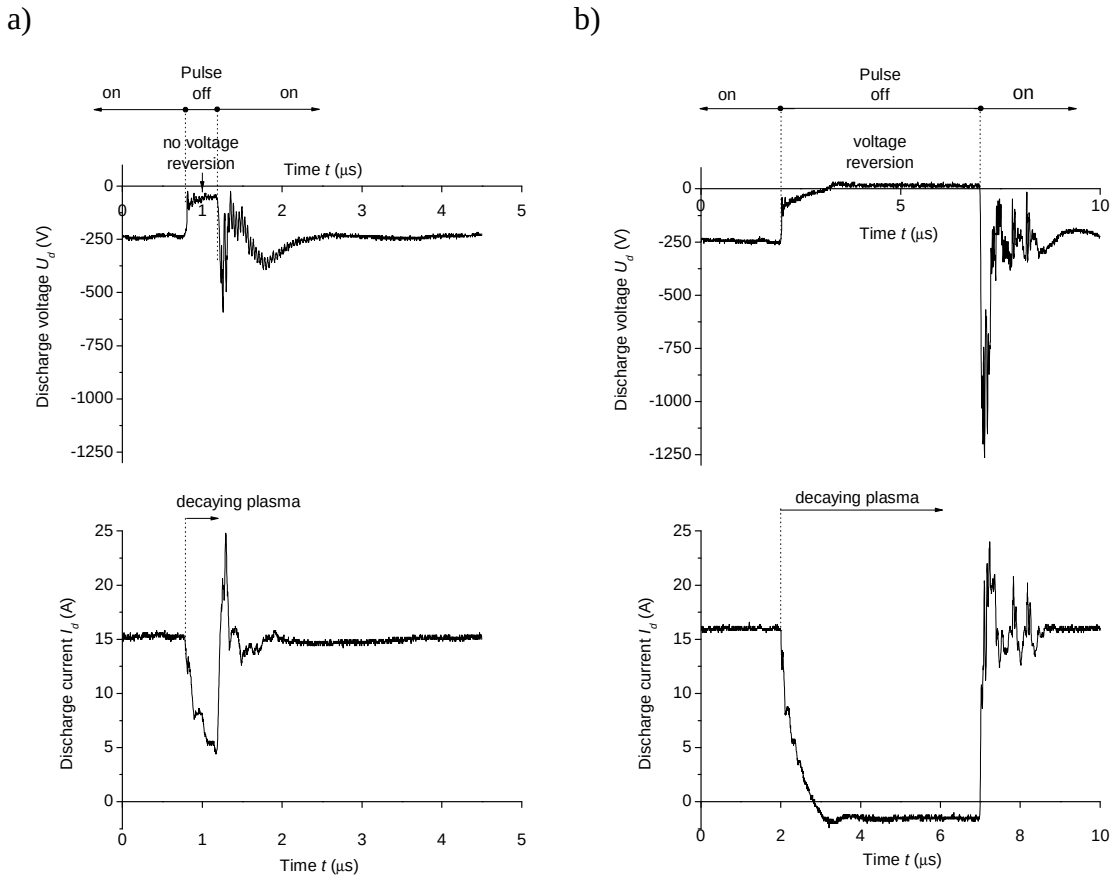

Figure 5.2.2. Effect of the length of pulse-off time (a) t_{off} = 0.4 μs and (b) t_{off} = 5.0 μs in DC pulse reactive single magnetron sputtering of alumina film at f_r = 5 kHz and W_{ta} = 50 W/cm^2 on time evolution of discharge voltage $U_d(t)$ and discharge current $I_d(t)$ waveforms.

Once the pulse is switched off the ion current flow decreases, i.e. the plasma decays. Here the rate of decay depends on the PPS output impedance, gas mixture composition and pressure at the moment.

If the pulse-off time t_{off} is too short, in our case t_{off} = 0.4 μs (Figure 5.2.2.a waveforms on the left) arcs occur (detected and counted by PPS) and the deposition process becomes unstable. The arcs are also visible by naked eye through the glass feedthrough of the vacuum chamber. These arcs occur because the discharge current has not enough

time to convert from the ion current to the electron current. Such a short time does not allow the PPS to turn the discharge voltage to a positive value (10% of |Ud|) which could attract the electrons from the target vicinity. This lack of electron flow on the target surface causes that the positive charge accumulated on the target during the pulse-on time is not neutralized by the electrons and an arc occurs after reaching the breakdown. Reaching this breakdown does not have to occur immediately after starting the deposition process. This fact will be proven later. The time of first arc occurence depends on (i) the PPS pulsing parameters influencing the charging and discharging of the insulating layer, (ii) target power density influencing the deposition rate of the insulating layer on the uneroded target area and (iii) sputtering gas and its pressure influencing the resputtering of the insulating layer.

Once the pulse-off time is increased to t_{off} = 5 μs (Figure 5.2.2.b waveforms on the right) the plasma decay has enough time for converting the ion current to the electron current attracted by the positive target voltage. Then the accumulated positive charge on the target surface is neutralized by the electrons. No arcing occured during this deposition even at the lowest f_r = 5kHz.

5.2.3. Effect of target power density W_{ta} on process stability

Situation described above is devoted to the high target power density W_{ta} = 50 W/cm^2. The next step was to investigate the influence of the different target power density W_{ta} on the transient phenomena during the shortest pulse-off time t_{off} = 0.4 μs. Evolution of U_d and I_d during the pulse-off time at f_r = 5 kHz and W_{ta} = 10, 20, 30, 40 and 50 W/cm^2 is shown in the Figure 5.2.3.

The ion current is converted to the electron current only in weak magnetron discharges at $W_{ta} \leq$ 10 W/cm^2. Therefore accumulated positive charge is removed and the reactive sputtering of alumina thin films runs without the arcing. On the contrary the arcing occurs in enhanced discharges generated at W_{ta} > 10 W/cm^2 because no electron current flows on the target surface because of a longer time of plasma decay. Longer plasma decay is caused by higher ionization of the sputtering gas. Therefore the accumulated charge at the target surface can not be removed during short t_{off} = 0.4 μs.

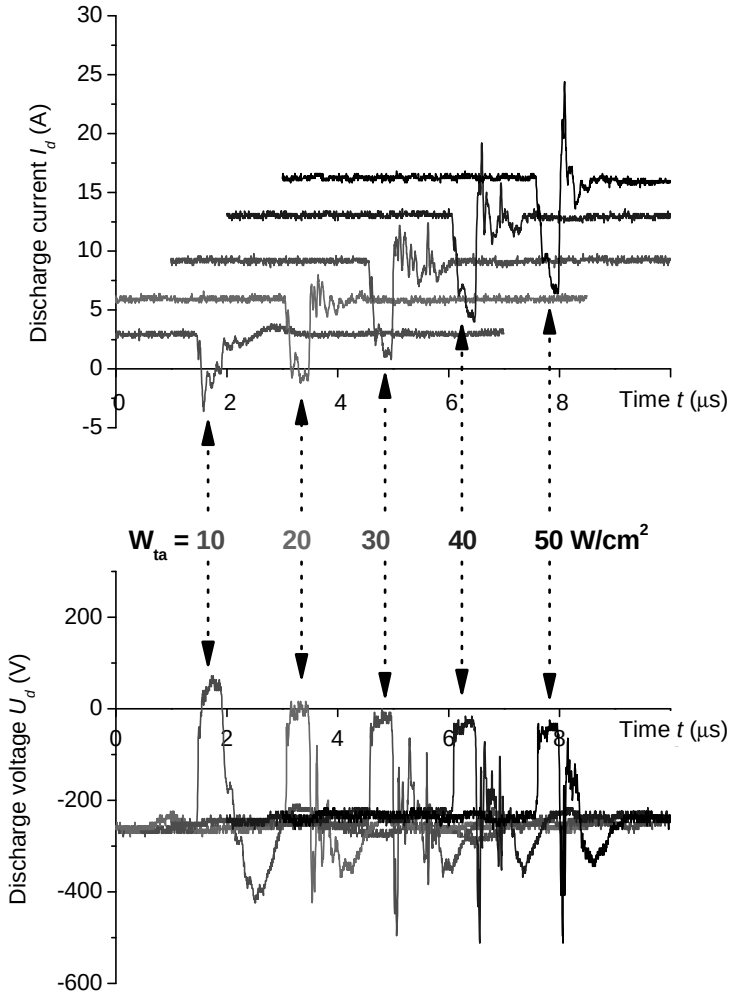

Figure 5.2.3. Evolution of $U_d(t)$ and $I_d(t)$ in the pulse-off time interval of single magnetron discharge generated by Advanced Energy PPS at f_r = 5 kHz, t_{off} = 0.4 μs with target power density W_{ta} increasing from 10 to 50 W/cm^2.

5.2.4. Effect of high repetition frequency f_r on process stability

Discussion above is devoted to the lowest repetition frequency f_r = 5 kHz. When f_r was increased to 100 kHz the deposition process was again stable when pulse-off time t_{off} was sufficiently long, i.e. t_{off} = 5 μs. However when t_{off} was decreased to the lowest value t_{off} = 0.4 μs the sputtering was not stable and arcing occured even at this high repetition frequency. The explanation is the same as for the lowest f_r = 5 kHz. The discharge voltage does not reach positive value during t_{off} = 0.4 μs, therefore the ion

current is not converted into the electron current and no positive charge neutralization occurs. Waveforms for f_r = 100 kHz and both t_{off} = 0.4 μs and 5.0 μs at W_{ta} = 30W/cm^2 are shown in the Figure 5.2.4.

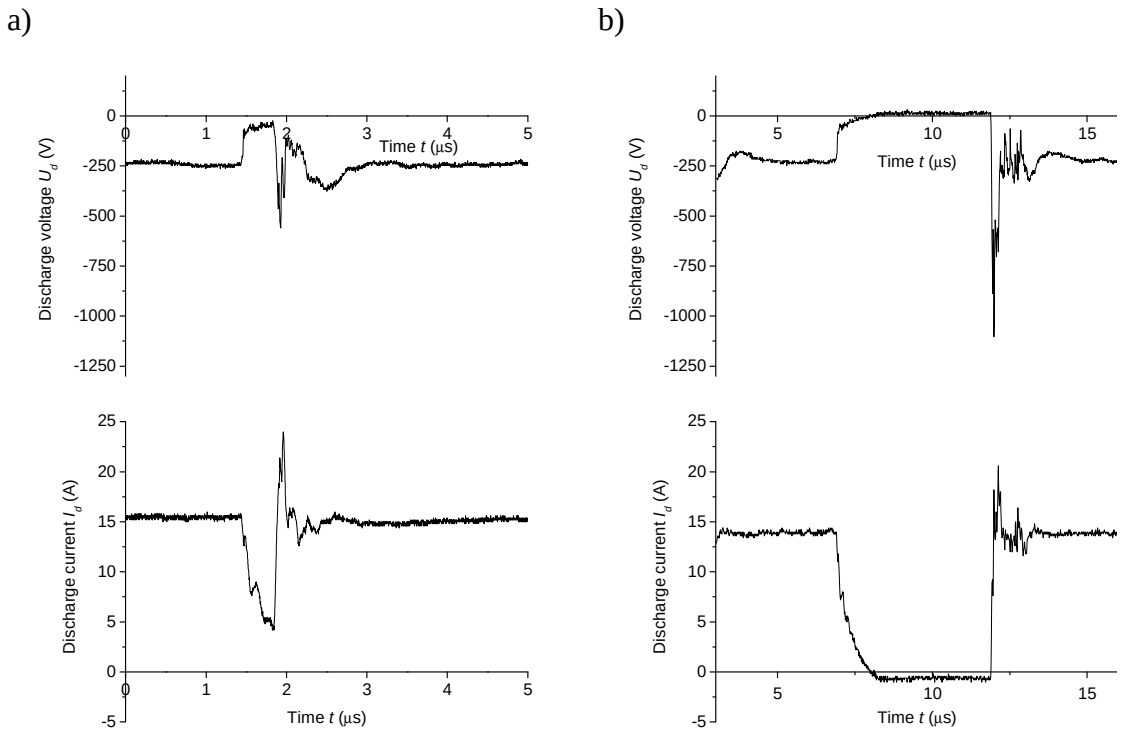

Figure 5.2.4. Effect of the length of pulse-off time (a) t_{off} = 0.4 μs and (b) t_{off} = 5.0 μs in DC pulse reactive single magnetron sputtering of alumina film at f_r = 100 kHz and W_{ta} = 30 W/cm^2 on time evolution of discharge voltage $U_d(t)$ and discharge current $I_d(t)$ waveforms.

It is clearly seen that a simple increase of f_r is not a sufficient condition to avoid the arcing. Pulse-off time t_{off} must be sufficiently long for converting the ion current to the electron current. Also used W_{ta} and gas pressure p are important parameters influencing the plasma decay during the t_{off}. All these facts need to be considered in the design of pulse power supplies.

5.2.5. Cummulative arc counts evolution

The Advanced Energy PPS is able to detect, suppress and count the arcs which occur during the deposition process. The detection principle is schematically shown in the Figure 4.2.3. The voltage drops and the current increases at the very begining of the arc, both rapidly. The actuall voltage is monitored by the arc detection feature of the Advanced Energy PPS. The arc detection level was set to -50 V for most of the experiments. Once the discharge voltage suddenly drops on the detection value the arc is detected, counted and the discharge is switched off.

When the PPS parameters are set such a way that the sputtering process purposely becomes unstable it does not have to happen immediately after starting the deposition. So called cummulative arc time evolution at different W_{ta} and different f_r is illustrated in the Figure 5.2.5. below.

Following can be concluded:

- It takes several minutes when first arc occurs depending on the deposition conditions mainly on W_{ta} and PPS parameters.
- The evolution of the arc counts follows exponential trend.
- The exponential growth of counts is probably caused by increasing the thickness of insulating layer deposited on uneroded target areas i.e. increasing the probability of the insulating layer breakdown.

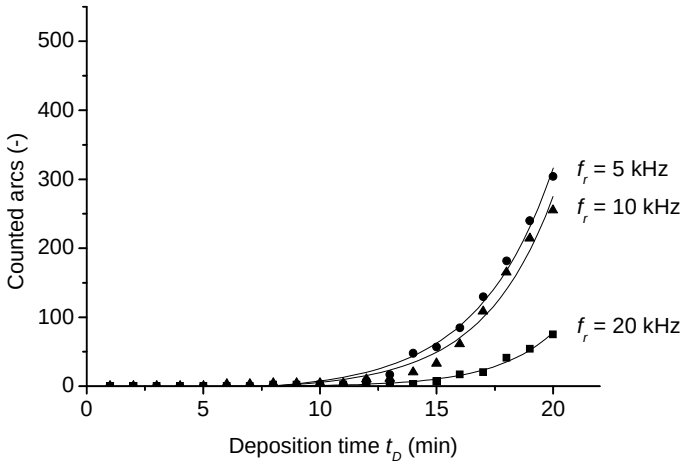

Figure 5.2.5. Number of counted arcs during the deposition time t_D at different low repetition frequencies f_r = 5, 10 and 20 kHz and at target power density W_{ta} = 50 W/cm^2.

5.2.6. Arc detection level effect

The Advanced Energy PPS can detect, count and suppress the arcs which occur during the reactive sputtering process. The schematic principle is shown in the Chapter 4.2. All the experiments mentioned above were performed with the arc detection level set at -50V. Short experiment with different arc detection level was performed. Two Al_2O_3 films were deposited at known unstable deposition conditions, i.e. at W_{ta} = 50 W/cm^2, f_r = 5kHz and t_{off} = 0.4 μs. One thin film was deposited with arc detection level -50V. Second film was deposited with arc detection level -100V. Pictures of the film surface acquired by the light microscope are shown in the Figure 5.2.6. below.

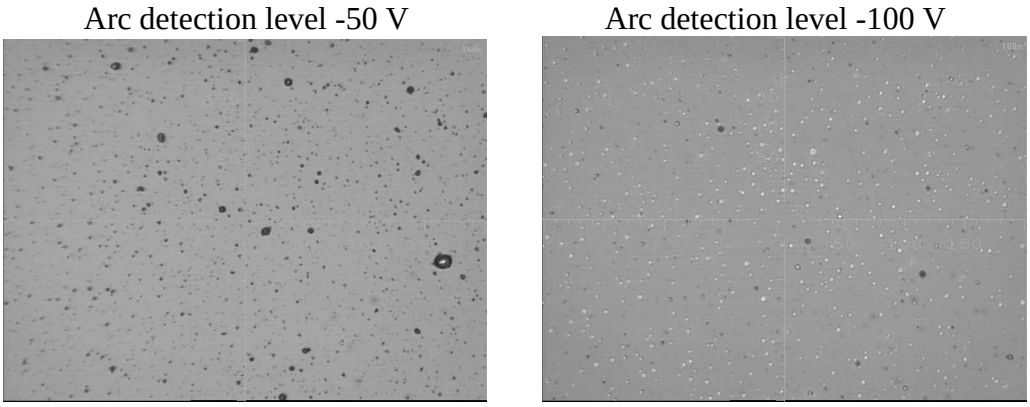

Figure 5.2.6. Illustration of the effect of the arc detection level of Advanced Energy PPS in DC pulse reactive single magnetron sputtering of alumina film at f_r = 5 and 100 kHz and W_{ta} = 50W/cm^2 on its surface morphology. Images were acquired by the light microscope.

Larger macroparticles in the Al_2O_3 film were found during the deposition with the lower arc detection level -50 V than the macroparticles released during the process with higher arc detection level -100 V. The explanation can be following:

- The discharge voltage during the pulse-on time was typically -250 V for both experiments.
- Once an arc occured during the deposition with -50 V arc detection level the potential difference of this arc was 200 V when detected and before the discharge was switched off. On the contrary arc with potential difference 150 V occured during higher arc detection level -100 V. In other words arc

detected at U_d = -50 V has a higher energy which can cause releasing of larger macroparticles from the target, see the Figure 5.2.6. above.

5.2.7. Surface quality of Al_2O_3 films

There are several significant consequences of arcing during the reactive sputtering:

1. the target lifetime is reduced during intensive arcing,
2. the deposition process is unstable because of switching off the discharge,
3. the power supply electronics can be damaged
4. and the growing film is damaged by macroparticles released from the target.

The surface quality of the growing alumina film is discussed below. The Figure 5.2.7. shows pictures of the Al_2O_3 surface of the films prepared at high target power density W_{ta} = 50W/cm^2 when a different repetition frequency f_r = 5 and 100 kHz and pulse-off time t_{off} = 0.4 and 5.0 μs were applied. Pictures below were acquired by the light microscope.

Following information can be concluded from the pictures:

- The surface of the Al_2O_3 film is smooth without macroparticles at f_r = 5 kHz and t_{off} = 5.0 μs because no arcs occured during this deposition process. This is caused by the sufficiently long pulse-off time t_{off} = 5 μs. The ion current was converted in the electron current which resulted in an efficient neutralization of the positive charge accumulated on the target surface.
- On the other hand a lot of macroparticles released by the arcing can be found in the Al_2O_3 film deposited at the same repetition frequency f_r = 5 kHz but at short pulse-off time t_{off} = 0.4 μs. There was no electron current which would neutralize the accumulated positive charge on the target surface.
- Very same situation was observed when Al_2O_3 films were sputtered at f_r = 100 kHz at long and short pulse-off time t_{off} = 5.0 μs and 0.4 μs respectively. No arcing, i.e. no surface defects were found on the Al_2O_3 surface when the pulse-off time was sufficiently long. Once the pulse-off time was too short arcs

occured resulting in releasing the macroparticles from the target surface and impacting the growing alumina film.

Analysis by the scanning electron microscope (SEM) equipped with the energy dispersive spectrometer (EDS) was performed. Smooth surface of the Al_2O_3 film prepared at stable conditions without the arcing, i.e. f_r = 5 kHz and t_{off} = 5.0 μs is shown in the Figure 5.2.8.a. On the contrary Al_2O_3 surface with macroparticles produced during unstable conditions with the arcing, i.e. f_r = 5 kHz and t_{off} = 0.4 μs is shown in the Figure 5.2.8.b.

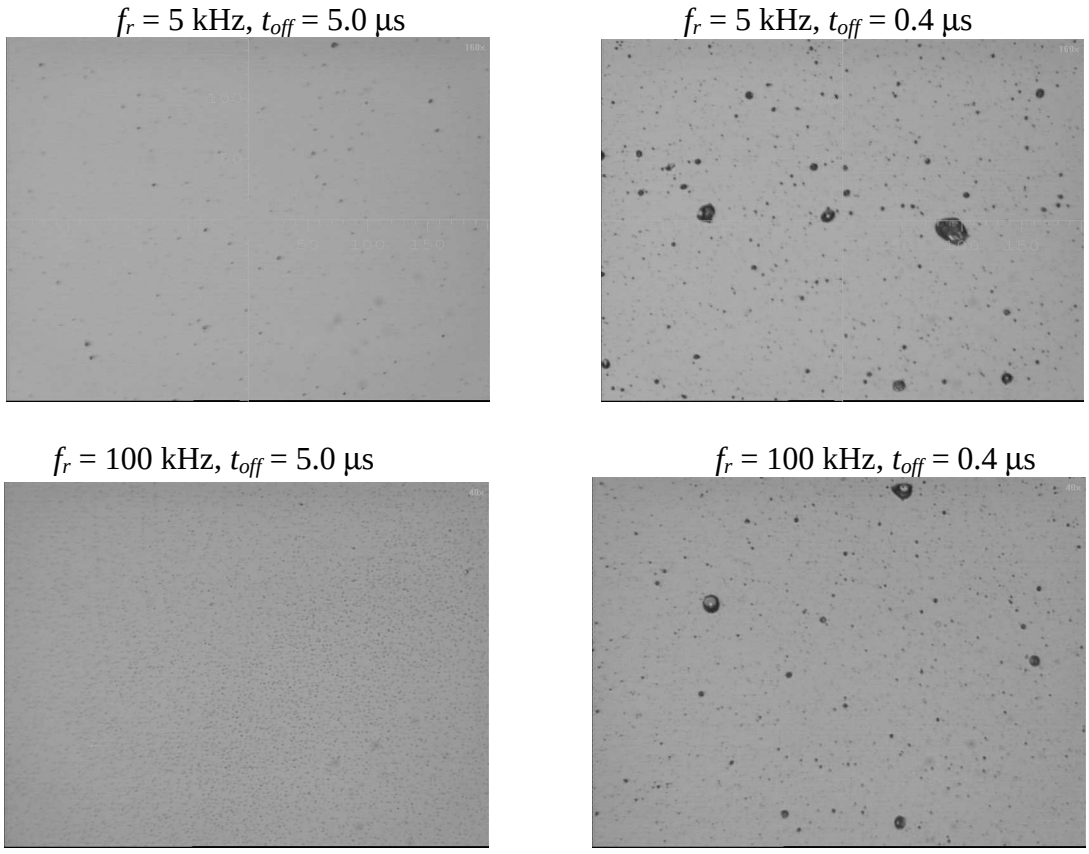

Figure 5.2.7. Illustration of the effect of the length of pulse-off time t_{off} in DC pulse reactive single magnetron sputtering of alumina film at f_r = 5 and 100 kHz and W_{ta} = 50W/cm^2 on its surface morphology. Images were acquired by light microscope.

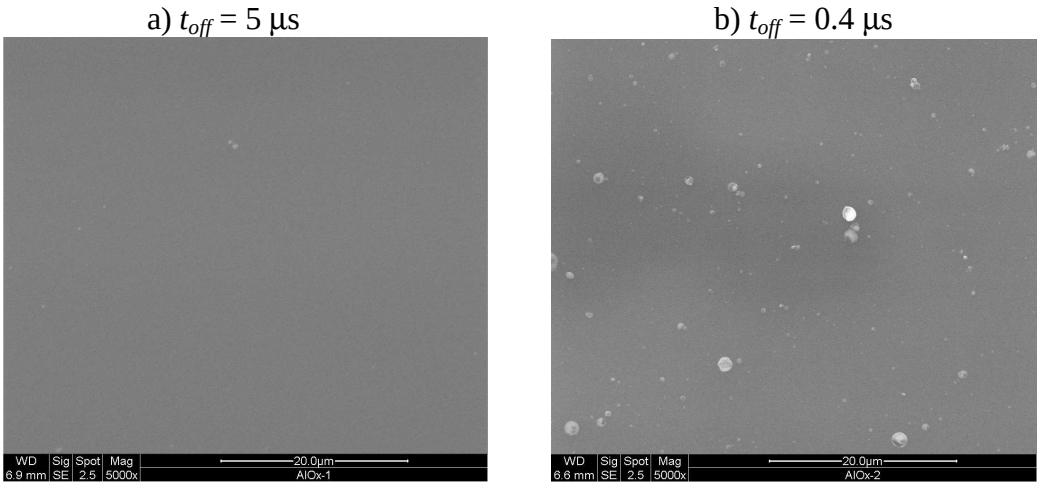

Figure 5.2.8. Illustration of the effect of the length of pulse-off time t_{off} in DC pulse reactive single magnetron sputtering of alumina film at f_r = 5 kHz and W_{ta} = 50W/cm^2 on its surface morphology. Images were acquired by SEM.

Qualitative EDS analysis revealed the macroparticles consist mainly of the aluminium, i.e. from the target material.

It was shown that increasing the repetition frequency f_r is not a sufficient condition for the arc-free DC pulse reactive magnetron sputtering of Al_2O_3 thin films. Also the pulse length τ, target power density W_{ta} and pulse-off time t_{off} play an important role. It was also shown that alumina films undamaged by the arcing can be prepared at low repetition frequencies f_r at high duty cycles up to τ/T = 97.5%, i.e. at high deposition rates a_D if W_{ta} does not overpass the value where the accumulated charge reaches the breakdown. The main results were also reported here [106].

5.3. Two-phase Al-O-N nanocomposite thin films

Single layer Al-O-N thin films were prepared by DC pulse reactive magnetron sputtering using a dual unbalanced magnetron equipped by pure metallic Al targets sputtered in a mixture of oxygen and nitrogen where the oxygen was injected in pulses. Phase and elemental composition together with mechanical properties like hardness *H*, Young's modulus *E*, elastic recovery W_e, stress σ and resistance to cracking of Al-O-N films are discussed in detail.

The following Table 5.3.1. summarizes the deposition conditions at which the Al-O-N thin films were deposited.

Table 5.3.1. Deposition conditions for reactive magnetron sputtering of Al-O-N thin films

Deposition parameter	**Value**
Partial nitrogen pressure p_{N2}	1 Pa
Nitrogen flow ϕ_{N2}	27 sccm (constant)
Partial oxygen pressure p_{O2}	Pulse
Oxygen flow ϕ_{O2}	5 sccm in a pulse
Substrate-to-target distance $d_{S\text{-}T}$	100 mm
Discharge current I_{da}	3 A
PPS repetition frequency f_r	100 kHz
PPS duty cycle τ/T	0.5
Target power density W_{da}	11 W/cm^2
Substrate potential U_S	U_{fl} (floating potential)
Substrate temperature T_S	RT; 500°C
Oxygen pulse-on time τ_{O2}	2 s
Oxygen pulsing period T_{O2}	0 – 40 s

5.3.1. Oxygen pulses

The nitrogen flow was set to a constant flow ϕ_{N2} = 27 sccm to get the nitrogen partial pressure $p_{N2} \approx 1$ Pa during all the depositions. The oxygen was injected in pulses during the deposition process. The oxygen pulse-on time τ_{O2} was constant for all the depositions i.e. τ_{O2} = 2 s. This time was selected empirically as the optimum – long enough to let the electronics and flowmeter respond on the signal from PC and short enough to inject only a small amount of oxygen to avoid a dominant target poisoning by oxygen. The deposition process was controlled by varying the oxygen pulsing period

T_{O2}. Oxygen pulses and total pressure behaviour are shown in the Figure 5.3.1. Short oxygen pulses result in partial oxygen pressure $p_{O2} \approx 0.05$ Pa in a pulse. The total pressure was not controlled at a constant value.

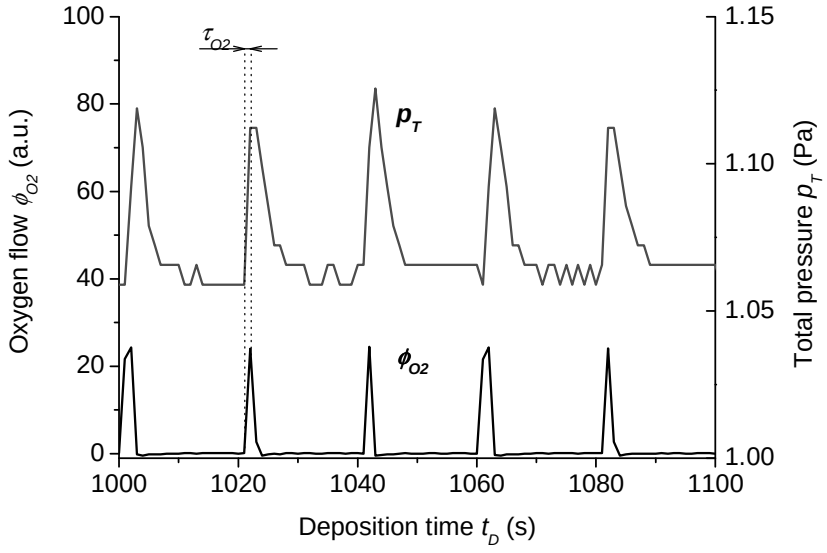

Figure 5.3.1. Oxygen flow pulses and total pressure behaviour when oxygen injected in pulses at ϕ_{O2} = 2 sccm, τ_{O2} = 2 s and T_{O2} = 20 s during the deposition of Al-O-N film at a constant nitrogen flow ϕ_{N2} = 27 sccm.

5.3.2. Al-O-N films on glass substrate

5.3.2.1. Phase composition

The phase composition of the Al-O-N films on glass substrate prepared at different oxygen pulsing periods T_{O2} at T_S = RT and 500°C was evaluated by XRD, see the Figure 5.3.2. below.

The structure of the films deposited on unheated glass substrate (T_S = RT) evolved as follows:

- at τ_{O2}/T_{O2} = 0 (i.e. no oxygen introduced) polycrystalline AlN film with dominant (002) crystal plane was produced,
- at T_{O2} = 40 to 20 s polycrystalline AlN films were produced,
- at T_{O2} = 15 s very weak nanocrystalline AlN reflection was found

- and at T_{O2} < 15 s x-ray amorphous Al-O-N films were produced.

XRD analysis of the films deposited on substrate heated at T_S = 500°C revealed following information:

- When no oxygen was introduced (τ_{O2}/T_{O2} = 0) again the polycrystalline AlN film with dominant (002) plane was produced, similar situation as for the film deposited on unheated substrate.
- With T_{O2} decreasing from 40 s to 15 s the crystalline AlN structure is continuously suppressed to a nanocrystalline AlN structure.
- At T_{O2} = 10 s x-ray amorphous Al-O-N film is produced.
- At T_{O2} = 2 s (i.e. at continuous oxygen introduction) XRD indicated weak nanocrystalline γ-Al_2O_3 reflection.

The data above show that:

- The oxygen pulsing period T_{O2} has a strong influence on the structure of Al-O-N thin films.
- The crystallization of AlN is suppressed with decreasing T_{O2}, i.e. with increasing the amount of oxygen in the sputtering gas mixture during the oxygen pulse period.
- Lower crystallinity of AlN (see the lower intensities of x-ray reflections in the Figure 5.3.2.) was found out for the films deposited on heated substrate at T_S = 500°C compared to the films deposited on unheated substrate. This can be due to the release of the oxygen from the chamber walls, enhanced dissociation of oxygen molecules and incorporation of the oxygen into the Al-O-N matrix resulting in a formation of higher content of x-ray amorphous Al_2O_3 phase in the growing thin film.
- When oxygen was introduced continuously without pulsing the film deposited on unheated substrate was x-ray amorphous. On the other hand the film deposited on heated substrate at T_S = 500°C showed weak nanocrystalline γ-Al_2O_3 reflection. This is due to a higher energy delivered to the growing film by heating the substrate.

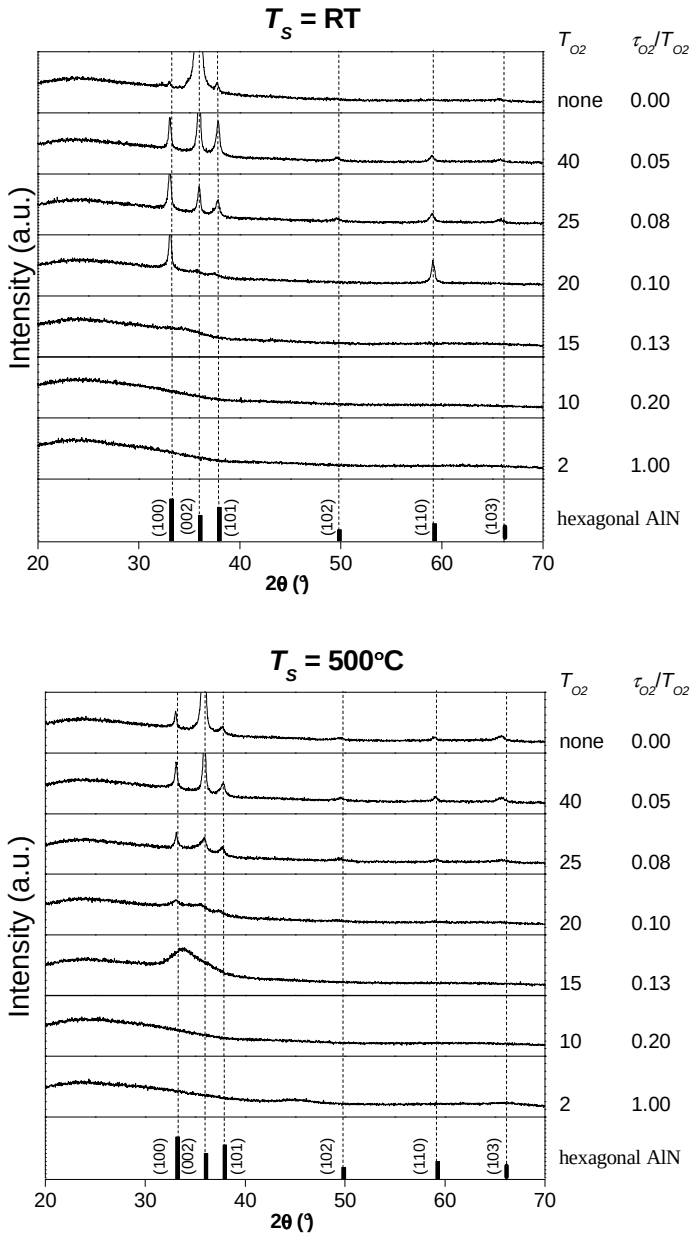

Figure 5.3.2. XRD patterns of Al-O-N thin films on glass substrate prepared at different oxygen pulsing period T_{O2} at T_S = RT and 500°C respectively.

Later it will be also shown even the films deposited with no oxygen flow contain some oxygen revealed by XRF. This is due to the presence of residual oxygen after pumping down the system and due to the oxygen molecules released from the vacuum chamber walls.

5.3.2.2. Elemental composition

Following Table 5.3.2. and Figure 5.3.3. show the elemental composition of the films prepared both on unheated and heated glass substrates.

Table 5.3.2. Elemental composition of Al-O-N thin films on glass substrate prepared at different oxygen pulsing period T_{O2} at T_S = RT and 500°C respectively.

T_S = RT				
T_{O2} (s)	τ_{O2}/T_{O2}	Al (at.%)	O (at.%)	N (at.%)
∞	0.00	49.0	12.3	38.6
40	0.05	48.2	15.0	36.8
25	0.08	48.6	14.7	36.7
20	0.10	47.0	14.6	38.4
15	0.13	42.7	26.1	31.2
10	0.20	39.3	50.5	10.2
2	1.00	39.7	60.3	0.0
T_S = 500°C				
T_{O2} (s)	τ_{O2}/T_{O2}	Al (at.%)	O (at.%)	N (at.%)
∞	0.00	47.9	12.6	39.5
40	0.05	n.m.	n.m.	n.m.
25	0.08	49.7	12.6	37.7
20	0.10	48.8	15.1	35.9
15	0.13	44.3	24.8	30.9
10	0.20	37.0	46.6	16.4
2	1.00	36.9	62.8	0.3

When the oxygen duty cycle τ_{O2}/T_{O2} is increased i.e. the oxygen portion in the sputtering gas mixture is increased the oxygen content in the Al-O-N films increases as well. Simultaneously the nitrogen content decreases. The aluminium content slightly decreases.

Films prepared at τ_{O2}/T_{O2} = 0 i.e. when no oxygen was introduced into the sputtering gas the films contains ~ 12 at.% of oxygen. This is caused by the residual oxygen gas after pumping down the vacuum chamber as already mentioned above.

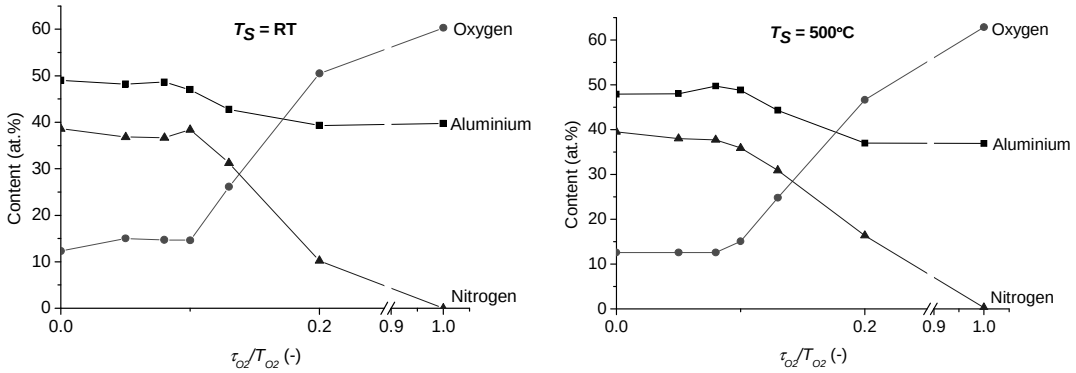

Figure 5.3.3. Elemental composition determined by XRF of Al-O-N thin films on glass substrate prepared at different oxygen pulsing period T_{O2} at T_S = RT (on the left) and 500°C (on the right) respectively.

5.3.2.3. Mechanical properties

Mechanical properties of Al-O-N films prepared at different oxygen pulsing parameters on unheated and heated glass substrate were determined. Table 5.3.3. summarizes the hardness H, Young's modulus E^*, ratio H/E^* and elastic recovery W_e. Here W_e and H/E^* represents the mechanical behaviour of the film [97, 98]. The ratios of the hardness to Young's modulus (either H/E^* or H^3/E^{*2}) are proportional to the resistance of the material to the plastic deformation. This relation has been found out and confirmed for Al-Cu-O thin films [100] and Zr-Al-O thin films [99].

These mechanical properties were evaluated by the Vickers microindentation method described in the Chapter 4.4.7. Maximum load L = 30 mN was used for all the measurements.

The mechanical properties are strongly influenced by varying the oxygen pulsing duty cycle τ_{O2}/T_{O2} see the Figure 5.3.4. above.

- Lowest hardness H together with the lowest elastic recovery W_e and the lowest ratio H/E^* exhibits the film with crystalline AlN structure (see the XRD pattern in the Figure 5.3.2.) which was deposited without the oxygen injection during the deposition i.e. at τ_{O2}/T_{O2} = 0.
- While introducing the oxygen with increasing the oxygen pulsing duty cycle τ_{O2}/T_{O2} from 0.05 to 0.13 the mechanical properties are enhancing. The best mechanical properties, i.e. hardness H from ~14 to ~18 GPa, elastic recovery

W_e > 60% and ratio H/E^* > 0.1 were found for the films with nanocrystalline structure.

- The films prepared at τ_{O2}/T_{O2} = 0.2 are x-ray amorphous and exhibit lower values of the discussed mechanical properties compared with nanocrystalline films.
- Film deposited at T_S = 500°C with continuous oxygen introduction (i.e. τ_{O2}/T_{O2} = 1) exhibits good mechanical properties i.e. H = 17.5 GPa, H/E^* = 0.133 and W_e = 74.3 %. This is due to the nanocrystallization of γ-Al_2O_3 revealed by XRD. The film deposited at the same τ_{O2}/T_{O2} = 1 but on the unheated substrate did not exhibit such enhancement of the mechanical properties because of x-ray amorphous structure of the film.

Table 5.3.3. Mechanical properties of Al-O-N thin films on glass substrate prepared at different oxygen pulsing period T_{O2} at T_S = RT and 500°C respectively.

T_S = RT					
τ_{O2}/T_{O2} (-)	h (nm)	H (GPa)	E^* (GPa)	H/E^* (-)	W_e (%)
0.00	3100	6.7	108.7	0.062	45.3
0.05	2600	8.9	117.2	0.076	52.9
0.08	2900	10.5	121.4	0.086	57.6
0.10	3100	15.5	127.9	0.121	66.8
0.13	2900	13.8	108.0	0.128	65.0
0.20	2500	9.7	104.0	0.093	53.2
1.00	1200	10.8	93.4	0.116	59.7
T_S = 500°C					
τ_{O2}/T_{O2} (-)	h (nm)	H (GPa)	E^* (GPa)	H/E^* (-)	W_e (%)
0.00	2700	6.5	106	0.061	47.4
0.05	2600	8.7	115	0.076	55.5
0.08	2300	7.2	70	0.103	57.8
0.10	2500	18.4	127	0.145	73.9
0.13	2700	18.3	117	0.156	79.0
0.20	2700	9.6	100	0.096	53.7
1.00	1900	17.5	132	0.133	74.3

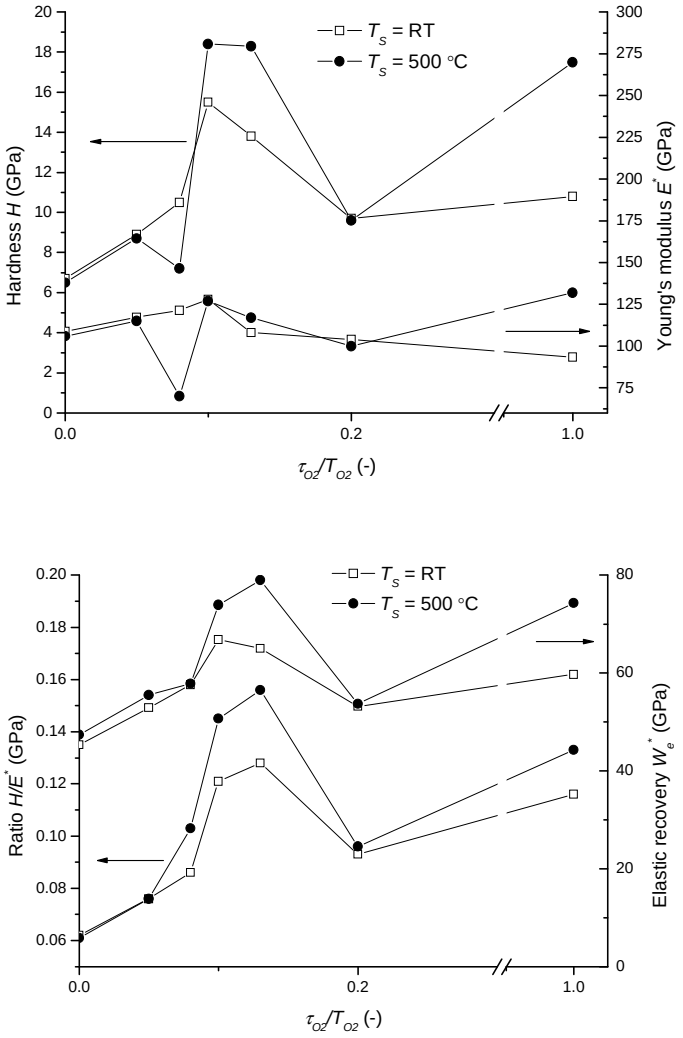

Figure 5.3.4. Mechanical properties – hardness H, Young´s modulus E^*, ratio H/E^* and elastic recovery W_e –of Al-O-N thin films on glass substrate prepared at different oxygen pulsing period T_{O2} at T_S = RT (on the left) and 500°C (on the right) respectively.

The substrate temperature T_S has a strong influence on the final mechanical properties as shown above. Heating the substrate at T_S = 500°C enhances the mechanical properties by:

- stimulating the nanocrystallization of AlN in the x-ray amorphous Al-O-N matrix, see the films deposited at τ_{O2}/T_{O2} = 0.10 and 0.13

- and by delivering the energy to the nanocrystallization of γ-Al_2O_3 embedded into Al-O-N x-ray amorphous matrix by heating the substrate when oxygen is introduced continuously, see the film deposited at $\tau_{O2}/T_{O2} = 1$.

5.3.3. Al-O-N films on silicon and molybdenum substrate

Serie of the Al-O-N films deposited on Si (100) and molybdenum substrate heated at T_S = 500°C was prepared with finer steps of τ_{O2}/T_{O2} (i) to get more detailed information about the evolution of structure and mechanical properties and (ii) to evaluate the resistance to cracking of Al-O-N films on molybdenum substrate.

5.3.3.1. Phase composition

Following can be concluded from the XRD patterns of Al-O-N films on silicon substrate shown in the Figure 5.3.5.:

- Crystalline AlN structure of the film deposited without the oxygen introduction ($\tau_{O2}/T_{O2} = \infty$) was suppressed when the oxygen was introduced in pulses.
- Nanocrystallization of AlN occured for τ_{O2}/T_{O2} increasing up to 0.167.
- The films deposited at τ_{O2}/T_{O2} = 0.200 and 0.250 are x-ray amorphous.
- Further increasing of τ_{O2}/T_{O2} caused increase in oxygen incorporation into the growing Al-O-N film.
- The nanocrystallization of γ-Al_2O_3 occured at $\tau_{O2}/T_{O2} \geq 0.333$.
- The structure evolution from crystalline AlN through nc-AlN/a-Al-O-N and x-ray amorphous Al-O-N to nc-γ-Al_2O_3/a-Al-O-N exhibit the same trend as for the films deposited on glass substrate.

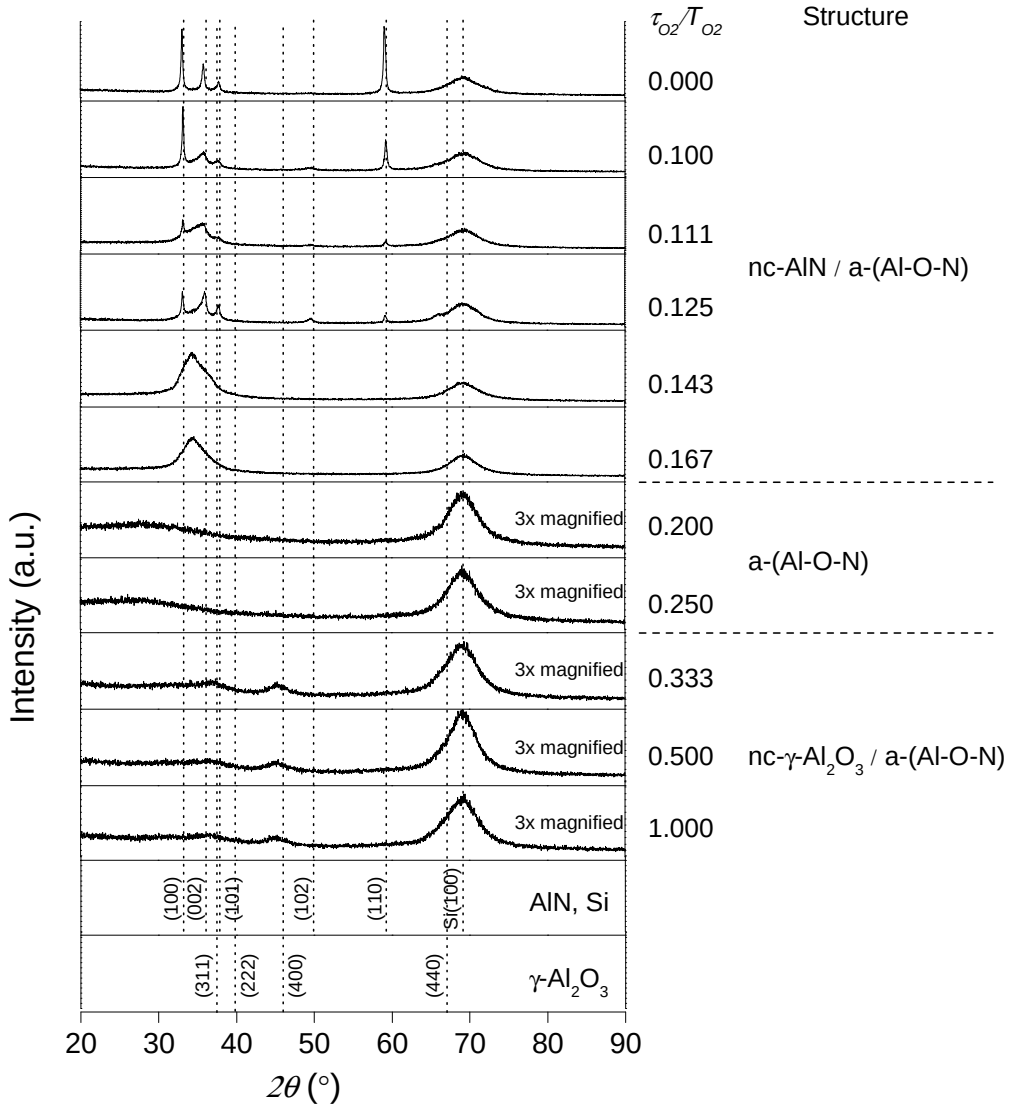

Figure 5.3.5. XRD patterns of Al-O-N thin films on Si (100) substrate prepared at different oxygen pulsing period T_{O2} at T_S = 500°C.

5.3.3.2. Mechanical properties

Summary of mechanical properties is shown in the Table 5.3.4. followed by the trends in the Figure 5.3.6.

Table 5.3.4. Summary of mechanical properties and information about the structure of Al-O-N thin films on Si (100) substrate prepared at different oxygen pulsing period T_{O2} at T_S = 500°C.

τ_{O2}/T_{O2} (-)	h (nm)	H (GPa)	E^* (GPa)	H/E^* (-)	W_e (%)	Stress σ (GPa)	*Structure*
0.000	2900	9.6	138	0.07	50	-0.47	c-AlN/a-(Al-O-N)
0.100	2900	16.1	160	0.101	62	-0.50	nc-AlN/a-(Al-O-N)
0.111	2900	17.3	150	0.115	67	-0.55	
0.125	2700	15.3	160	0.096	62	-0.43	
0.143	2700	18.4	136	0.135	75	-0.58	
0.167	3300	18.2	135	0.135	74	na	
0.200	2900	10.8	122	0.089	52	-0.18	a-(Al-O-N)
0.250	2800	9.9	119	0.083	50	-0.14	
0.333	1700	18.6	173	0.108	66	-1.60	nc-Al_2O_3/a-(Al-O-N)
0.500	1500	20.3	176	0.115	69	-2.20	
1.000	1700	18.3	172	0.106	67	-2.10	

The lowest values of the mechanical properties were found again for „pure“ AlN film and for the films with x-ray amorphous structure i.e. at τ_{O2}/T_{O2} = 0 and 0.20 ÷ 0.25 respectively.

The highest values of the hardness H, elastic recovery W_e and ratio H/E^* were found for those films with nanocrystalline structure either with nc-AlN or nc-Al_2O_3 both embedded in x-ray amorphous Al-O-N matrix.

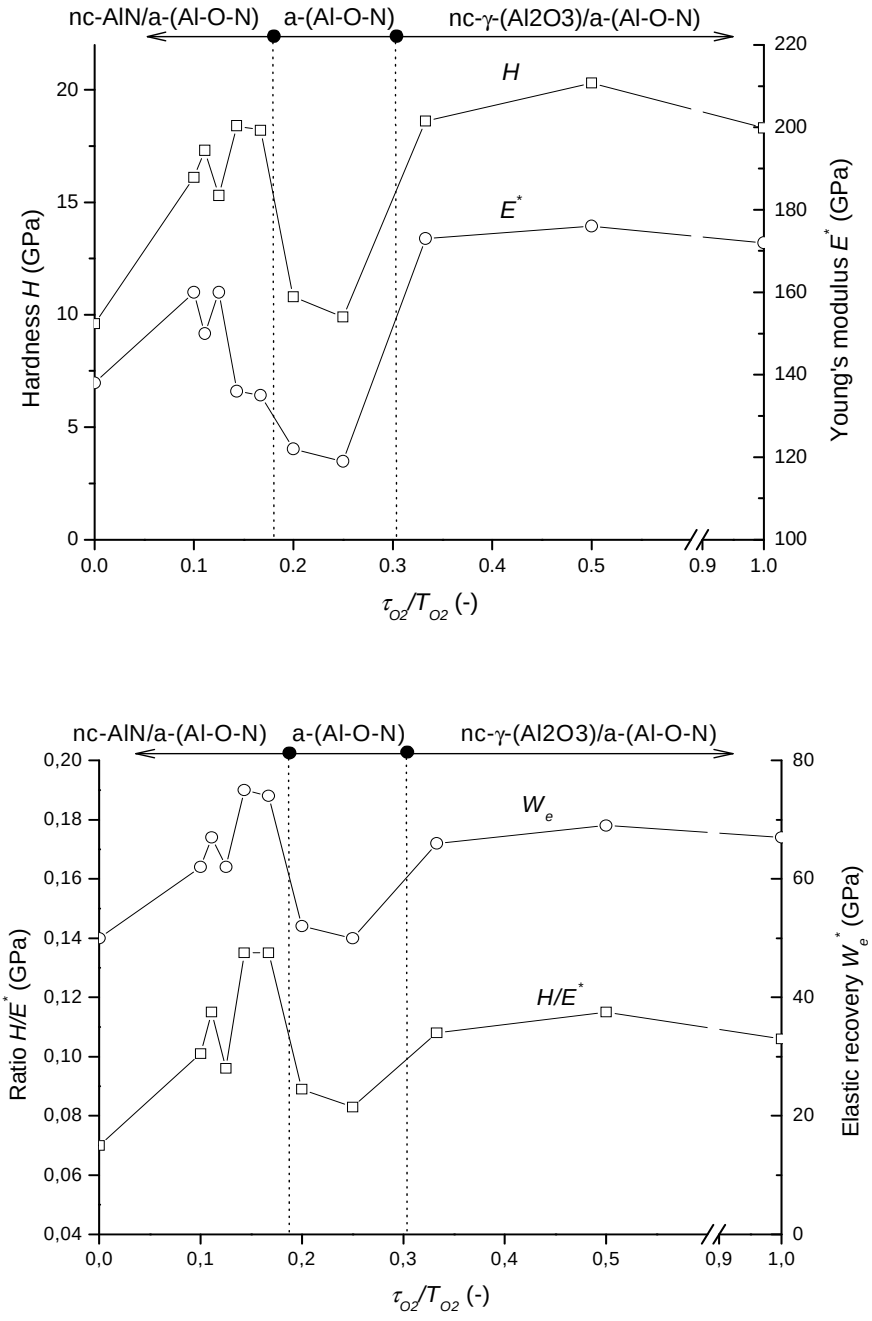

Figure 5.3.6. Mechanical properties of Al-O-N thin films on Si (100) substrate prepared at different oxygen pulsing period T_{O2} at T_S = 500°C.

5.3.3.3. Resistance to cracking

Part of this study was also to investigate the resistance of the films to cracking in bending and correlate this behaviour with the film structure measured by x-ray diffraction and with mechanical properties evaluated by the Vickers microindentation method. It was already mentioned that currently there is no unified standard measurement method for the evaluation of resistance to cracking. Inspired by the application (e.g. flexible electronics industry) resistance to cracking can be evaluated by bending the thin film on a suitable substrate along a cylinder with the defined diameter. Such a method assumes the films with a very good adhesion to the substrate. As our experience has shown during the years DC pulse reactive magnetron sputtering of metallic targets leads to a very good adhesion of the sputtered thin films on a variety of substrates.

The resistance to cracking of Al-O-N thin films deposited at different oxygen pulsing periods T_{O2} on heated molybdenum substrate at T_S = 500°C was studied. Structure and mechanical properties of these films are discussed above. Thin aluminium foil was used to protect the Al-O-N film from the direct contact with the cylinder over which the films were bent. Cylinder with 25 mm in diameter was used for all the bending experiments. Surface of the Al-O-N film was analyzed under the light microscope for any cracks after bending at the defined bending angle α_B. Capillary effect of the black marker was used for highlighting the cracks.

Pictures in the Figure 5.3.7. below represent the Al-O-N film surface either with no cracks before and after the bending and with cracks after the bending.

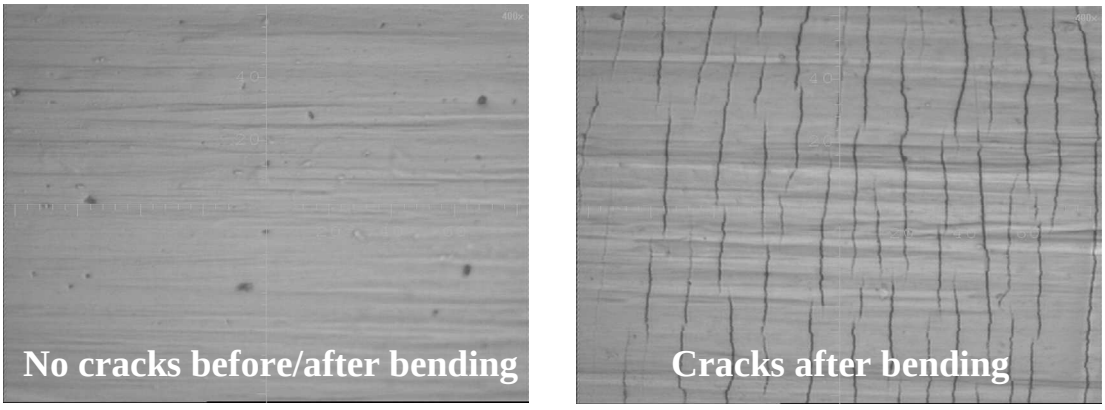

Figure 5.3.7. Pictures of Al-O-N films on molybdenum substrate acquired by optical microscope before and after the bending.

The bending results are summarized together with mechanical properties and information about the structure in the Table 5.3.5. below.

Table 5.3.5. Summary of mechanical properties, structure and bending results of Al-O-N thin films prepared at different oxygen pulsing period T_{O2} at T_S = 500°C.

τ_{O2}/T_{O2} (-)	H (GPa)	E^* (GPa)	H/E^* (-)	W_e (%)	Structure	Bending [2]
0.000	9.6	138	0.07	50	c-AlN/a-(Al-O-N)[1]	No cracks
0.100	16.1	160	0.101	62	nc-AlN/a-(Al-O-N)	Cracks at α_C = 40°
0.111	17.3	150	0.115	67		No cracks
0.125	15.3	160	0.096	62		Cracks at α_C = 40°
0.143	18.4	136	0.135	75		No cracks
0.167	18.2	135	0.135	74		No cracks
0.200	10.8	122	0.089	52	a-(Al-O-N)	Cracks at α_C = 40°
0.250	9.9	119	0.083	50		No cracks
0.333	18.6	173	0.108	66	nc-Al_2O_3/a-(Al-O-N)	No cracks
0.500	20.3	176	0.115	69		No cracks
1.000	18.3	172	0.106	67		Not measured [3]

[1] During this deposition no oxygen was introduced into the sputtering gas mixture. However the oxygen is present in the film in Al-O-N matrix where the oxygen comes from the residual atmosphere and from the chamber walls.

[2] Bending was performed up to α_B = 180°. Once first cracks occured a critical bending angle α_C was noted.

[3] No bending experiment was performed due to the thin film delamination.

The films with nanocrystalline nitride or oxide phase and exhibiting a relatively high ratio $H/E^* > 0.1$ are resistant to cracking in bending up to the bending angle α_B = 180° along the cylinder with the diameter of 25 mm. Similar correlation was obtained for Zr-Al-O thin films see [99] for reference.

However in some cases even films with low ratio $H/E^* < 0.1$ and low elastic recovery $W_e \approx 50\%$ exhibit no cracks up to α_B = 180°. As an example crystalline AlN film sputtered when no oxygen was introduced to the sputtering gas mixture exhibited such

resistance to cracking. The reason of no cracks occurence under given conditions is not clear. XRD pattern and XRF data show crystalline AlN phase and oxygen incorporated due to a residual atmosphere after the pumping respectively. This can indicate that also the amount of the individual phases in the composite film can controll the resistance to cracking. However such theory should be confirmed by more detail investigation, not in the scope of this thesis.

6. Conclusions

This Ph.D. thesis is devoted to reactive magnetron sputtering of oxide based and oxynitride nanocomposite thin films. The main results of this thesis can be briefly summarized as follows:

Two-functional DC sputtered TiO_2/Cu nanocomposite thin films

1. The optical properties like the optical band gap E_g and transmittance T strongly depends on TiO_2/Cu film structure. The film structure is controlled either by the deposition conditions like the partial oxygen pressure p_{O2}, total pressure p_T, substrate temperature T_S or by post-deposition thermal annealing defined by the annealing environment, annealing temperature T_a and time of annealing t_a. The latter means that the optical properties depend on the energy delivered to the growing film during thermal annealing. The variation of p_{O2}, p_T, T_S and/or T_a and t_a was used for the preparation of TiO_2/Cu thin films with different optical properties.
2. Hydrophilic behaviour was found for nanocrystalline TiO_2/Cu film with low copper content ~1.5 at.%. This film exhibits low water droplet contact angle (WDCA) $\alpha \approx 20°$ even without the UV irradiation.
3. The incorporation of copper into the nanocrystalline anatase TiO_2 thin film can result in a strong antibacterial effect induced by UV irradiation. The exact copper content should be optimized to obtain the strongest antibacterial effect. Optimized nanocrystalline TiO_2/Cu thin film with low copper content ~ 1.5 at.% exhibited a rapid killing of *Escherichia Coli* bacteria already after UV irradiation for 20 minutes only.
4. Transparent anatase nanocrystalline TiO_2/Cu film with low copper content ~ 1.5 at.% shows simultaneously two functions induced by UV irradiation: (i) good hydrophilicity with WDCA $\alpha \leq 20°$ and (ii) strong antibacterial effect by killing the *Escherichia Coli* bacteria.

Elimination of arcing in reactive sputtering of Al_2O_3 thin films

1. Increasing the repetition frequency f_r is not a sufficient condition to suppress the arcing during DC pulse reactive magnetron sputtering. Also the pulse-off time t_{off} and transient phenomena during t_{off}, pulse length τ and pulse target power density W_{ta} are of key importance.

2. Optimized choice of W_{ta}, τ and t_{off} must be selected to avoid the arcing. W_{ta} is limited by the length of pulse τ to avoid the accumulation of positive charge over the breakdown value during pulse-on time τ. Also t_{off} must be sufficiently long for converting the ion current I_i to the electron current I_e and for complete discharge of accumulated positive charge on the target surface prior to the next pulse.

3. The highest repetition frequency f_r which can be used for arc-free high power pulse magnetron sputtering (W_{ta} >> 100 W/cm^2) with duty cycle $\tau/T \geq 0.5$ will be determined by a sufficiently long t_{off}. The length of pulse-off time t_{off} is of key importance for the elimination of arcing in a pulse reactive sputtering of electrically insulating compounds.

4. Single magnetron was used for the arc-free pulse reactive sputtering of Al_2O_3 thin films even at low repetition frequency f_r = 5 kHz and relatively high target power density $W_{ta} \approx$ 50 W/cm^2 when t_{off} = 5 μs was selected. Here f_r = 5 kHz is the minimum repetition frequency and W_{ta} = 50 W/cm^2 is the maximum target power density of the used Advanced Energy pulse power supply respectively. Maximum value of W_{ta} for arc-free reactive sputtering needs to be determined.

5. Al_2O_3 thin films undamaged by arcing can be prepared at a low f_r and high duty cycle up to τ/T = 97.5%, i.e. at high deposition rates a_D if W_{ta} does not overpass a value at which the accumulated positive charge reaches the breakdown.

Two-phase Al-O-N nanocomposite thin films

1. Introducing the oxygen in pulses into nitrogen gas during the DC pulse reactive magnetron sputtering of two Al targets enables the growth of two kinds of single layer nanocrystalline composites: (i) nc-(AlN)/a-(Al-O-N) nanocomposite with lower oxygen content and (ii) nc-(γ-Al_2O_3)/a-(Al-O-N) with higher oxygen content. X-ray amorphous a-(Al-O-N) films are formed in the transition between

these two nanocomposites. The phase composition was controlled by varying the oxygen pulsing period T_{O2} at a constant oxygen pulse-on time τ_{O2} = 2 s.

2. Nanocrystalline phase grown in amorphous matrix strongly enhances the mechanical properties compared with the amorphous material. Both nanocomposites, i.e. nc-AlN/a-(Al-O-N) and nc-(γ-Al_2O_3)/a-(Al-O-N), exhibit relatively high hardness H = 15 – 20 GPa, low Young's modulus E^* satisfying the ratio H/E^* > 0.1 and high elastic recovery W_e > 60%. On the contrary x-ray amorphous a-(Al-O-N) thin films exhibit lower H ≈ 10 GPa, low ratio H/E^* < 0.1 and low W_e ≈ 50%.
3. Hard nanocomposite thin films with higher ratio i.e. H/E^* > 0.1 deposited on molybdenum strips exhibit good resistance to cracking in bending.
4. Nanocrystalline Al-O-N nanocomposite thin films with hardness H = 15 – 20 GPa, ratio H/E^* > 0.1 and elastic recovery W_e > 60% deposited on 0.1 mm thick molybdenum strip with no cracks in the film during bending along the fixed cylinder with 25 mm in diameter up to α_B = 180° of bending angle were successfully prepared.

7. References

[1] A. Fujishima, K. Honda, Nature 238 (1972) 37.

[2] A. Fujishima, X. Zhang, Comptes Rendus Chimie 9 (2006) 750.

[3] M. Anpo, M. Takeuchi, Jounal of Catal. 216 (2003) 505.

[4] U. Diebold, Surf. Sci. Rep. 48 (2003) 53.

[5] N.Sakai, A. Fujishima, T. Watanabe, K. Hashimoto, J. Phys. Chem. B 105 (2001) 3023.

[6] M. Meissner, *Reactive magnetron sputtering of photoactive TiO_2 thin films and their properties*, Diploma thesis, Department of Physics, University of West Bohemia, Pilsen, Czech Republic (2007).

[7] T. Kameda, K. Ohkuma, N. Sano, N. Batbayar, Y. Terashima, K. Terada, Orthodontic Waves 73 (2014) 55.

[8] H. Junli, W. Li, R. Nanqi, M. Fang, Juli, Wat. Res. Vol. 31 (1997) 607.

[9] K.K. Jyoti, A.B. Pandit, Biochem. Eng. J. 18 (2004) 9.

[10] G. Lu, Ch. Li, Y. Zheng, Q. Zhang, J. Peng, M. Fu, J. Photochem. Photobiol. B: Biol. 92 (2008) 42.

[11] D. G. Ribeiro, A. C. Pavarinaa, L. N. Dovigo, D. M. P. Spolidorio, E. T. Giampaolo, C. E. Vergani, J. Dentistry 37 (2009) 666.

[12] T. Ohshima, K. Okuyama, M. Sato, J. Electrostatics 55 (2002) 227.

[13] J.J. Cotter, P. Maguire, F. Soberon, S. Daniels, J.P. O'Gara, E. Casey, J. Hospital Infection 78 (2011) 204.

[14] H.A. Foster, I.B. Ditta, S. Varghese, A. Steele, Appl. Microbiol. Biotechnol. 90 (2011) 1847.

[15] S.A. Wilks, H. Michels, C.W. Keevil, Int. J. Food Microbiol. 105 (2005) 445.

[16] L.A. Brook, P. Evans, H.A. Foster, M.E. Pemble, A. Steele, D.W. Sheel, H.M. Yates, J. Photochem. Photobiol. A: Chemistry 187 (2007) 53.

[17] H.A. Foster, D.W. Sheel, P. Sheel, P. Evans, S. Varghese, N. Rutschke, H.M. Yates, J. Photochem. Photobiol. A: Chemistry 216 (2010) 283.

[18] X. Zhang, X. Huang, Y. Ma, N. Lin, A. Fan, B. Tang, Appl. Surf. Sci. 258 (2012) 10058.

[19] V. Ondok, J. Musil, M. Meissner, R. Čerstvý, K. Fajfrlík, J. Photochem. Photobiol. A: Chemistry 209 (2010) 158.

[20] J. Musil, M. Louda, R. Čerstvý, P. Baroch, I.B. Ditta, A. Steele, H.A. Foster, Nanoscale Research Letters 4 (2009) 313.

[21] J. Šícha, J. Musil, M. Meissner, R. Čerstvý, Appl. Surf. Sci. 254 (2008) 3793.

[22] A. Fujishima, T. N. Rao, D. A. Tryk, J. Photochem. Photobiol. C: Photochemistry Reviews 1 (2000) 1.

[23] Y. Kikuchi, K. Sunada, T. Iyoda, K. Hashimoto, A. Fujishima, J Photochem. Photobiol. A: Chemistry 106 (1997) 51.

[24] M. Sokmen, F. Candan, Z. Sumer, J. Photochem. Photobiol. A: Chemistry 143 (2001) 241.

[25] K. Sunada, T. Watanabe, K. Hashimoto, J. Photochem. Photobiol. A: Chemistry 156 (2003) 227.

[26] N. Sakai, A. Fujishima, T. Watanabe, K. Hashimoto, J. Phys. Chem. B 105 (2001) 3023.

[27] B. Alberts, et al., Essential Cell Biology, 1998, Czech Edition.

[28] T. Sato, M. Taya, Biochem. Eng. J. 30 (2006) 199.

[29] C.H. Griffiths, H.K. Eastwood, J. Appl. Phys. 45 (1974) 2201.

[30] L.A. Brook, P. Evans, H.A. Foster, M.E. Pemble, D.W. Sheel, A. Steele, H.M. Yates, Surf. Coat. Technol. 201 (2007) 9373.

[31] www.pilkington.com

[32] J.H. Hsieh, T.H. Yeh, C.S. Chiou, C.T. Huang, C. Li, Adv. Sci. Technol 66 (2010) 142.

[33] J.H. Hsieh, T.H. Yeh, S.Y. Hung, S.Y. Chang, W. Wu, C. Li, Mat. Res. Bull. 47 (2012) 2999.

[34] J. Musil, J. Blažek, K. Fajfrlík, R. Čerstvý, Š. Prokšová, Appl. Surf. Sci. 276 (2013) 660.

[35] O. Baghriche, J. Kiwi, C. Pulgarin, R. Sanjines, J. Photochem. Photobiol. A: Chemistry 229 (2012) 39.

[36] X. B. Tian, Z. M. Wang, S. Q. Yang, Surf. Coat. Technol. 201 (2007) 8606.

[37] I. Safi, Surf. Coat. Technol. 127 (2000) 203.

[38] J. Musil, P. Baroch, J. Vlček, K. H. Nam, J. G. Han, Thin Solid Films 475 (2005) 208.

[39] J. Musil, *Physical and mechanical properties of hard nanocomposite films prepared by magnetron sputtering*, Chapter 10 in *Nanostructured hard coatings*, Kluwer Academic (2005).

[40] J. Musil, J. Vlček, Surf. Coat. Technol. 112 (1999) 162.

[41] J. Musil, J. Vlček, P. Baroch, *Magnetron discharges for thin films plasma processing* in *Materials surface processing by directed energy techniques*, Elsevier (2006), 67.

[42] P. Baroch, *Reactive magnetron sputtering of film based on Ti*, Ph.D. thesis, Department of Physics, University of West Bohemia, Pilsen, Czech Republic (2004).

[43] U. Krause, M. List, H. Fuchs, Thin Solid Films 392 (2001) 196.

[44] C. Mitterer, O. Heuze, V.-H. Derflinger, Surf. Coat. Technol. 89 (1997) 233.

[45] K. Koski, J. Hölsä, P. Juliet, Surf. Coat. Technol. 115 (1999) 163.

[46] A. Belkind, A. Freilich, R. Scholl, Surf. Coat. Technol. 108 – 109 (1998), 558.

[47] L.Sirghi, T.Aoki, Y.Hatanaka, Thin Solid Films 422 (2002) 55.

[48] I. N. Reddy, V. Rajagopal Reddy, N. Sridhara, V. S. Rao, M. Bhattacharya, P. Bandyopadhyay, S. Basavaraja, A. K. Mukhopadhyay, A. K. Sharma, A. Deya, Ceramics International 40 (2014) 9571.

[49] S. C. B. Gopinath, T.-H. Tang, Y. Chen, M. Citartan, T. Lakshmipriya, Biosensors and Bioelectronics 60 (2014) 332.

[50] M. Wright, T. Beardow, J. Vac. Sci. Technol. A4 (1986) 388.

[51] M. Vergöhl, D. Rademacher, A. Pflug, Surf. Coat. Technol. 241 (2014) 38.

[52] S. Maniv, C. Miner, W.D. Westwood, J. Vac. Sci. Technol. 18 (1981) 195.

[53] I. Safi, Surf. Coat. Technol. 135 (2000) 48.

[54] S. Schiller, U. Heisig, Chr. Korndorfer, G. Beister, J. Reschke, K. Steinfelder, J. Strumpfel, Surf. Coat. Technol. 49 (1987) 405.

[55] P. J. Kelly, P. S. Henderson, R. D. Arnell, G. A. Roche, D. Carter, J. Vac. Sci. Technol. A 18 (2000) 208.

[56] X. Yu, X. Yang, Ch.-B. Wang, M. Hua, Z.-Q. Fu, Surf. Coat. Technol. 228 (2013) 519.

[57] J. Xiong, Y. Xia, Y. Xue, F. Zhang, P. Guo, X. Zhao, B. Tao, Physica C 497 (2014) 38.

[58] J. Musil, P. Baroch, Vacuum 87 (2013) 96.

[59] J. Vlček, J. Rezek, J. Houška, R. Čerstvý, R. Bugyi, Surf. Coat. Technol. 236 (2013) 550.

[60] A. A. Solovyev, N. S. Sochugov, S. V. Rabotkin, A. V. Shipilova, I. V. Ionov, A. N. Kovalchuk, A. O. Borduleva, Appl. Surf. Sci. 310 (2014) 272.

[61] X. Dong, Z. Wu, X. Xu, T. Wang, Y. Jiang, Vacuum 104 (2014) 97.

[62] V. Godinho, V. N. Denisov, B. N. Mavrin, N. N. Novikova, E. A. Vinogradov, V. A. Yakovlev, C. Fernandez-Ramos, M. C. Jimenez de Haro, A. Fernandez, Appl. Surf. Sci. 256 (2009) 156.

[63] J. Dong, P. Du, X. Zhang, Thin Solid Films 545 (2013) 414.

[64] A. Rizzo, M. A. Signore, L. Mirenghi, A. Cappello, L. Tapfer, Surf. Coat. Technol. 204 (2010) 2019.

[65] M. A. Signore, A. Rizzo, L. Mirenghi, M. A. Tagliente, A. Cappello, Thin Solid Films 515 (2007) 6798.

[66] J. M. Chappé, N. Martin, J. Lintymer, F. Sthal, G. Terwagne, J. Takadoum, Appl. Surf. Sci. 253 (2007) 5312.

[67] S. Venkataraj, H. Kittur, R. Drese, M. Wuttig, Thin Solid Films 514 (2006) 1.

[68] H. Le. Dréo, O. Banakh, H. Keppner, P.-A. Steinmann, D. Briand, N. F. de Rooij, Thin Solid Films 515 (2006) 952.

[69] M. Grafouté, C. Petitjean, C. Rousselot, J.F. Pierson, J. M. Greneche, Scripta Mater. 56 (2007) 153.

[70] C. Petitjean, M. Grafouté, C. Rousselot, J.F. Pierson, Surf. Coat. Technol. 202 (2008) 4825.

[71] M. Fenker, H. Kappl, C. S. Sandu, Surf. Coat. Technol. 202 (2008) 2358.

[72] J. M. Chappé, P. Carvalho, F. Vaz, M. Fenker, H. Kappl, N. M. G. Parreira, A. Cavaleiro, E. Alves, Surf. Coat. Technol. 202 (2008) 2363.

[73] M. Fenker, H. Kappl, P. Carvalho, F. Vaz, Thin Solid Films 519 (2011) 2457.

[74] F. Richard, F. Hickernell, F. Cho, US Patent US4701008, 1987.

[75] J. Probst, U. Gbureck, R. Thull, Surf. Coat. Technol. 148 (2001) 226.

[76] P. Wilhartitz, S. Dreer, P. Ramminger, Thin Solid Films 447 – 448 (2004) 289.

[77] R. Mientus, R. Grötschel, K. Ellmer, Surf. Coat. Technol. 200 (2005) 341.

[78] C. Nunes, V. Teixeira, M. L. Prates, N. P. Barradas, A. D. Sequeira, Thin Solid Films 442 (2003) 173.

[79] S. Khamseh, J. Alloys and Compounds 611 (2014) 249.

[80] J. W. McCauley, P. Patel, M. Chen, G. Gilde, E. Strassburger, B. Paliwl, K. T. Ramesh, D. P. Dandekar, J. Eur. Ceram. Soc. 29 (2009) 223.

[81] J. Yue, Y. Liu, W. Zhao, G. Li, Scr. Mater. 55 (2006) 895.

[82] T. M. Hartnett, S. D. Bernstein, E. A. Maguire, R. W. Tustison, Infrared Physics and Technol. 39 (1998) 203.

[83] K. R. Bray, R. L. C. Wu, S. Fries-Carr, J. Weimer, Thin Solid Films 518 (2009) 366.

[84] A. G. Erlat, B. M. Henry, J. J. Ingram, D. B. Mountain, A. McGuigan, R. P. Howson, C. R. M. Grovenor, G. A. D. Briggs, Y. Tsukahara, Thin Solid Films 388 (2001) 78.

[85] S. Dreer, R. Krismer, P. Wilhartitz, Thin Solid Films 354 (1999) 43.

[86] S. Dreer, R. Krismer, P. Wilhartitz, Surf. Coat. Technol. 114 (1999) 29.

[87] S. Dreer, P. Wilhartitz, E. Mersdorf, K. Piplits, G. Friedbacher, Mikrochim. Act. 131 (1999) 211.

[88] A. J. Aronson, D. Chen, W. H. Class, Thin Solid Films 72 (1980) 535.

[89] N. Martin, Ch. Rousselot, J. Vac. Sci. Technol. A 17 (1999) 2869.

[90] N. Martin, A. R. Bally, P. Hones, R. Sanjinés, F. Lévy, Thin Solid Films 377 – 378 (2000) 550.

[91] N. Martin, O. Banakh, A. M. E. Santo, S. Springer, R. Sanjinés, J. Takadoum, F. Lévy, Appl. Surf. Sci. 185 (2001) 123.

[92] N. Martin, R. Sanjinés, J. Takadoum, F. Lévy, Surf. Coat. Technol. 142 – 144 (2001) 615.

[93] N. Martin, J. Lintymer, J. Gaviolle, J. M. Chappé, F. Sthal, J. Takadoum, F. Vaz, L. Rebouta, Surf. Coat. Technol. 201 (2007) 7720.

[94] N. Martin, J. Lintymer, J. Gaviolle, J. M. Chappé, F. Sthal, J. Takadoum, F. Vaz, L. Rebouta, Surf. Coat. Technol. 201 (2007) 7727.

[95] N. Martin, J. Lintymer, J. Gaviolle, J. M. Chappé, F. Sthal, J. Takadoum, F. Vaz, L. Rebouta, Surf. Coat. Technol. 201 (2007) 7733.

[96] J. Musil, Surf. Coat. Technol. 207 (2012) 50.

[97] J. Musil, M. Jirout, Surf. Coat. Technol. 201 (2007) 5148.

[98] A. Leyland, A. Matthews, Surf. Coat. Technol. 177 – 178 (2004) 317.

[99] J. Musil, J. Sklenka, R. Čerstvý, Surf. Coat. Technol. 206 (2011) 2105.

[100] J. Blažek, J. Musil, P. Stupka, R. Čerstvý, J. Houška, Appl. Surf. Sci. 258 (2011) 1762.

[101] J. Musil, R. Jílek, M. Meissner, T. Tölg, R. Čerstvý, Surf. Coat. Technol. 206 (2012) 4230.

[102] www.advanced-energy.com

[103] V. Ondok, *Reactive magnetron sputtering of thin films*, Ph.D. thesis, Department of Physics, University of West Bohemia, Pilsen, Czech Republic (2008).

[104] http://www.ars.usda.gov

[105] M. Sreemany, S. Sen, Mater. Chem. Phys. 83 (2004) 169.

[106] M. Meissner, T. Tölg, P. Baroch, J. Musil, Plasma Process. Polym. 8 (2011) 500.

8. Publications and conferences

Publications

[I] J. Musil, R. Jílek, M. Meissner, T. Tölg, R. Čerstvý, *Two-phase single layer Al-O-N nanocomposite films with enhanced resistance to cracking*, Surf. Coat. Technol. 206 (2012) 4230.

[II] M. Meissner, T. Tölg, P. Baroch, J. Musil, *Elimination of arcing in reactive sputtering of Al_2O_3 thin films prepared by DC pulse single magnetron*, Plasma Process. Polym. 8 (2011) 500.

[III] V. Ondok, J. Musil, M. Meissner, R. Čerstvý, K. Fajfrlík, *Two-functional DC sputtered Cu-containing TiO_2 thin films*, J. Photochem. Photobiol. A: Chem. 209 (2010) 158.

[IV] J. Šícha, J. Musil, M. Meissner, R. Čerstvý, *Nanostructure of photocatalytic TiO_2 films sputtered at temperatures below 200°C*, Appl. Surf. Sci. 254 (2008) 3793.

Conferences (results presented personally)

[I] **M. Meissner**, J. Musil, T. Tölg, R. Jílek, R. Čerstvý, *Reactive magnetron sputtering of aluminium oxynitride thin films using pulse inlet of oxygen*, European Material Research Society 2011 Spring Meeting, May 9 – 13th 2011, Nice, France, poster presentation.

[II] **M. Meissner**, *Elimination of arcing in reactive DC pulse magnetron sputtering of Al_2O_3 thin films*, Potential and Applications of Surface Nanotreatment of Polymers and Glass 2010, October 25 – 27th 2010 Blansko, Czech Republic, oral presentation.

[III] **M. Meissner**, P. Baroch, J. Musil, *Suppression of arcing in DC pulse reactive magnetron sputtering*, 12th International Conference on Plasma Surface Engineering, September 13 – 17th 2010, Garmisch-Partenkirchen, Germany, poster presentation.

[IV] **M. Meissner**, J. Musil, P. Baroch, R. Čerstvý, *Two-functional DC sputtered Ag and Cu-containing TiO_2 thin films*, Potential and Applications of Nanotreatment of Medical Surfaces 2010, August 30th – September 1st 2010 Hejnice, Czech Republic, oral presentation.

[V] **M. Meissner**, J. Musil, R. Čerstvý, *Two-functional DC sputtered Cu-containing TiO_2 thin films*, Potential and Application of Thin Ceramic and Metal Coatings 2010, May 26 – 28th 2010, Pilsen, Czech Republic, oral presentation.

[VI] **M. Meissner**, V. Ondok, J. Musil, R. Čerstvý, K. Fajfrlík, *Two-Functional DC Sputtered Cu-Containing TiO_2 Thin Films*, 37th International Conference on Metallurgical Coatings and Thin Films, April 26 – 30th 2010, San Diego, USA, poster presentation.

[VII] **M. Meissner**, J. Musil, V. Ondok, K. Fajfrlík, *Two-functional DC magnetron sputtered Cu-containing TiO_2 thin films*, European Material Research Society 2009 Spring Meeting, June 8 – 12th 2009, Strasbourg, France, poster presentation.

[VIII] **M. Meissner**, J. Šícha, J. Musil, R. Čerstvý, *Nanostructure of photocatalytic TiO_2 films sputtered at temperatures below 200°C*, 23rd Symposium on Plasma Physics and Technology, June 16 – 19th 2008 Prague, Czech Republic, poster presentation.

Conferences (co-author)

[I] **R. Jílek**, M. Meissner, J. Musil, R. Čerstvý, *Reactive magnetron sputtering of aluminium oxynitride thin films using oxygen gas pulsing process*, 10th International Conference on Reactive Sputter Deposition, December 7 – 10th 2011, Linköping, Sweden, poster presentation (no personal participation).

[II] **R. Jílek**, M. Meissner, J. Musil, *Reactive magnetron sputtering of Al-O-N thin films using reactive gas pulsing*, Potential and Application of Thin Ceramic and Metal Coatings 2011, June 6 – 8th 2011, Pilsen, Czech Republic, oral presentation (personally attended).

[III] M. Meissner, **P. Baroch**, J. Musil, *Elimination of arcing in reactive DC pulse magnetron sputtering of Al_2O_3 thin films*, Magnetron Ion Processing Arcs

Technologies European Conference, June 15 – 18th 2010, Metz, France, poster presentation (no personal participation).

[IV] **J. Šícha**, P. Baroch, M. Meissner, R. Čerstvý, J. Musil, *Low temperature deposition of anatase TiO_2 films by dual magnetron sputtering*, 36th International Conference on Metallurgical Coatings and Thin Films, April 27 – May 1st 2009, San Diego, USA, oral presentation (no personal participation).

Annotation

This Ph.D. thesis is devoted to reactive magnetron sputtering of oxide based and oxynitride nanocomposite thin films. The work is divided into three thematic topics.

First part is devoted to the DC reactive magnetron sputtering of nanocomposite TiO_2/Cu thin films and their characterization. Here the main aim was to find the preparation conditions under which films exhibiting both hydrophilic behaviour and antibacterial effect after UV irradiation are formed. Discussed thin films were reactively sputtered from a composed Ti/Cu target in a mixture of oxygen and argon at a different total pressure p_T, partial oxygen pressure p_{O2} and substrate temperature T_S. Selected samples were also thermally annealed in a different environment at annealing temperature T_a and annealing time t_a. Such a way single layer nanocomposite TiO_2/Cu thin films with a different phase composition and copper content were prepared. Correlation between the optical properties, hydrophilic behaviour and efficiency of killing *Escherichia Coli* bacteria and phase composition and copper content is evaluated. It is shown that 1 μm thick nanocomposite TiO_2/Cu film with ~1.5 at.% of copper exhibits simultaneously both hydrophilicity with WDCA $\alpha \leq 20°$ and strong antibacterial effect on *Escherichia Coli* bacteria.

Second part of this thesis is reporting on the elimination of arcing during DC pulse reactive magnetron sputtering of Al_2O_3 thin films. Single unbalanced magnetron equipped with aluminium target was used for the experiments. Target was sputtered in a pure oxygen at total pressure p_T = 2 Pa and different target power densities W_{ta} ranging from ~10 to ~50 W/cm^2. The repetition frequency f_r, target power density W_{ta}, pulse-on time τ, pulse-off time t_{off} and transient phenomena during t_{off} are correlated with the arcing and surface quality of the sputtered alumina films. Alumina films damaged by the Al macroparticles released from the target surface during the arcing are presented. Increased repetition frequency is not a sufficient condition to avoid such arcing. It is shown that the pulse-off time t_{off} and transient phenomena during that time, pulse-on time τ and target power density W_{ta} are of key importance to suppress the arcing during DC pulse reactive magnetron sputtering of electrically insulating thin films. Smooth undamaged Al_2O_3 thin films were reactively sputtered even at the low f_r = 5 kHz, high duty cycle up to τ/T = 97.5% and relatively high $W_{ta} \approx 50$ W/cm^2.

Third part is dealing with two-phase nanocomposite Al-O-N thin films prepared by DC pulse reactive sputtering using the unbalanced dual magnetron. Aluminium targets were reactively sputtered in a mixture of nitrogen and oxygen where the oxygen was introduced in well defined pulses. This way two kinds of single layer nanocomposites with a wide range of the elemental composition were formed: (i) nc-AlN/a-(Al-O-N) and (ii) nc-(γ-Al_2O_3)/a-(Al-O-N). X-ray amorphous a-(Al-O-N) films were formed in the transition between two mentioned nanocomposite materials. The phase and elemental composition were controlled by the oxygen pulsing period T_{O2}. It is shown that nanocrystalline nitride or oxide phase embedded into amorphous Al-O-N matrix enhances the mechanical properties when compared to those with x-ray amorphous structure. Highly elastic thin films with nanocrystalline phase exhibit relatively high hardness H = 15 – 20 GPa, ratio H/E^* > 0.1, elastic recovery W_e > 60% and resistance to cracking in bending.

Anotace

Tato dizertační práce se věnuje reaktivnímu magnetronovému naprašování tenkých nanokompozitních vrstev na bázi oxidů a oxynitridů. Práce je rozdělena do tří tématických celků.

První část je věnována DC reaktivnímu magnetronovému naprašování nanokompozitních TiO_2/Cu tenkých vrstev a jejich charakterizaci. Hlavním cílem bylo nalezení podmínek, za kterých jsou připraveny vrstvy vykazující zároveň jak smáčivé chování, tak antibakteriální efekt po ultrafialovém ozařování. Diskutované tenké vrstvy byly reaktivně naprašovány ze složeného Ti/Cu terče ve směsi kyslíku a argonu za různého celkového tlaku p_T, parciálního tlaku kyslíku p_{O2} a teploty substrátu T_S. Vybrané vzorky byly také vyžíhány v různém prostředí při žíhací teplotě T_a během žíhacího času t_a. Touto cestou byly připraveny jednovrstevné nanokompozitní vrstvy TiO_2/Cu s různým fázovým složením a různým obsahem mědi. Je zde vyhodnocena korelace mezi optickými vlastnostmi, smáčivým chováním a efektivitou v zabíjení bakterie *Escherichia Coli* a fázovým složením a obsahem mědi ve vrstvách. Je ukázáno, že 1 μm silná nanokompozitní vrstva TiO_2/Cu s 1,5 at.% mědi vykazuje zároveň hydrofilní chování s kontaktním úhlem vodní kapky $\alpha \leq 20°$ a silným antibakteriálním účinkem prokázaným na *Escherichia Coli*.

Druhá část podává informace o eliminaci oblouků během DC pulzního reaktivního magnetronového naprašování tenkých vrstev Al_2O_3. Jeden nevyvážený magnetron vybavený hliníkovým terčem byl použit pro tyto experimenty. Terč byl rozprašován v čistém kyslíku za celkového tlaku p_T = 2 Pa a za různých výkonových hustot na terči W_{ta} v rozsahu mezi ~10 a ~50 W/cm^2. Opakovací frekvence f_r, výkonová hustota na terč W_{ta}, doba pulzu τ, doba vypnutí pulzu t_{off} a přechodové jevy během t_{off} jsou korelovány s oblouky a povrchovou kvalitou naprašovaných vrstev Al_2O_3. Jsou prezentovány vrstvy poškozené hliníkovými makročásticemi uvolněnými z terče během oblouků. Je ukázáno, že doba vypnutí pulzu t_{off} a přechodové jevy během této doby, délka pulzu τ a výkonová hustota na terči W_{ta} mají klíčový význam pro potlačení oblouků během DC pulzního reaktivního magnetronového naprašování elektricky nevodivých vrstev. Hladké nepoškozené vrstvy Al_2O_3 byly reaktivně naprašovány dokonce za nízké opakovací frekvence f_r = 5 kHz, vysokého pracovního cyklu až po τ/T = 97.5% a relativně vysoké výkonové hustoty $W_{ta} \approx$ 50 W/cm^2.

Třetí část se zabývá dvoufázovými nanokompozitními vrstvami Al-O-N připravenými DC pulzním reaktivním naprašováním nevyváženým duálním magnetronem. Hliníkové terče byly reaktivně rozprašovány ve směsi dusíku a kyslíku, kde kyslík byl připouštěn pulzně. Tímto způsobem byly připraveny dva druhy nanokompozitních vrstev v širokém rozsahu prvkového složení: (i) nk-AlN/a-(Al-O-N) a (ii) nk-(γ-Al_2O_3)/a-(Al-O-N). Röntgenově amorfní vrstvy a-(Al-O-N) byly připraveny na přechodu mezi výše zmíněnými nanokompozitními materiály. Fázové a prvkové složení vrstev bylo řízeno periodou pulzního napouštění kyslíku T_{O2}. Je ukázáno, že nanokrystalická nitridová nebo oxidová fáze zabudovaná do amorfní matrice zlepšuje mechanické vlastnosti vrstev ve srovnání s amorfními vrstvami. Vysoce elastické tenké vrstvy s nanokrystalickou fází vykazují poměrně vysokou tvrdost H = 15 – 20 GPa, poměr H/E^* > 0.1, elastickou vratnost W_e > 60% a odolnost proti praskání při ohybu.

Anotación

Esta tesis está dedicada al pulverizado de óxidos y oxinitruro de películas de nanocompuesto. El trabajo está dividido en tres partes.

La primer sección esta dedicada al pulverizando películas delgadas de nanocompuesto TiO_2/Cu por medio de una magnetron ractivo CD y su caracterizacion. Aquí, el objetivo

principal fue encontrar las condiciones bajo las cuales las películas exhibieron tanto un comportamiento hidrofílico como antibacterial una vez las radiaciones UV se forman. Las películas en cuestión fueron reactívamente pulverizadas desde una superficie de impacto compuesta por Ti/Cu inmerso en una mezcla de oxígeno y argón a diferente presión total $p_{T,}$ presión de oxígeno parcial p_{O2} y una temperatura de substrato T_S. Muestras seleccionadas también fueron anilladas en diferente ambiente a una temperatura de anillado T_a y tiempo de anillado t_a. De esta manera películas delgadas de capa sencilla de nanocompuesto TiO_2/Cu con diferente fase de composición y contenido de cobre fueron preparadas. La correlación entre propiedades ópticas, comportamiento hidrofílico y la eficiencia de eliminación de la bacteria *Escherichia Coli* y fases de composición y contenido de cobre es evaluada. Se muestra que una película gruesa de 1 μm de nanocompuesto de TiO_2/Cu con ~1.5 de % de cobre exhibe tanto la hidrofilicidad con WDCA $\alpha \leq 20°$ como un fuerte efecto antibacterial contra la *Escherichia Coli.*

La segunda sección describe la eliminación de arcos durante el pulso CD del magnetrón reactivo pulverizando películas delgadas de Al_2O_3. Un magnetrón sencillo no-balanceado equipado con superficie de impacto de aluminio fue utilizado para los experimentos. La superficie de impacto de sometió a oxígeno puro con una presión total p_T = 2 Pa y diferentes densidades de potencia W_{ta} variando entre ~10 a ~50 W/cm^2. La frecuencia de repetición f_r, densidad de potencia W_{ta}, tiempo de pulso-activo τ, tiempo de pulso-no-activo t_{off} y el fenómeno de trasciente durante t_{off} son correlacionados con el efecto de arco y la calidad de la superficie de las películas de alúmina pulverizadas. Las películas de alúmina se vieron afectadas por macropartículas de Al liberadas por la superficie de impacto durante la generación de arcos. El incremento de la frcuencia de repetición no es una medida suficiente para evitar la generación de dichos arcos. Se muestra que el pulso-no-activo t_{off} y el fenómeno de trasciente durante ese mismo tiempo, tiempo de pulso-activo τ y densidad de potencia W_{ta} son factores de suma importancia para suprimir el efecto de arco durante el pulso CD del magnetrón reactivo pulverizando películas delgadas eléctricamente. Películas de Al_2O_3 fueron reactívamente pulverizadas aún en baja f_r = 5 kHz, ciclo de trabajo hasta τ /T = 97.5% y una relativamente alta $W_{ta} \approx$ 50 W/cm^2.

En la tercera parte se discute sobre películas delgadas de nanocompuesto Al-O-N doble-fase elaborados por el pulso reactivo CD del pulverizado usando una magnetron dual no-balanceado. Blancos de aluminio fueron reactivamente pulverizados en una mezcla de nitrógeno y oxígeno donde el oxígeno fue introducido en pulsos bien definidos. De

esta manera dos tipos de nanocompuesto de capa sencilla con una amplio rango de la composición elemental fueron formados: (i) nc-AlN/a-(Al-O-N) y (ii) nc-(γ-Al_2O_3)/a-(Al-O-N). Películas a-(Al-O-N) de Rayos-X amorfos fueron formados en la trasnsición entre los dos nanocompuestos mencionados anteriormente. La fase y composición elemental fueron controladas por medio del período T_{O2} de injeccíon de oxígeno. Se muetra que nitruro nanocristalino o una fase de óxido incrustada en una matriz Al-O-N amorfa mejora las propiedades mecánicas cuando se comparan con aquellos con estructura de Rayos-X amorfa. Películas delgadas altamente elásticas con fase nanocristalina exhiben una dureza relativamente alta H = 15 – 20 GPa, proporción H/E^* > 0.1, recuperación elástica W_e > 60% y resistencia a la ruptura en doblamiento.